



## Modeling hysteresis in porous media flow via relaxation

B. Plohr<sup>a,b</sup>, D. Marchesin<sup>a</sup>, P. Bedrikovetsky<sup>c</sup> and P. Krause<sup>a</sup>

<sup>a</sup> *Instituto de Matemática Pura e Aplicada, Rio de Janeiro, RJ, Brazil*  
E-mail: {marchesi;krause}@fluid.impa.br

<sup>b</sup> *University at Stony Brook, Stony Brook, NY, USA*  
E-mail: plohr@ams.sunysb.edu

<sup>c</sup> *LENEP, Universidade Estadual do Norte Fluminense, Macaé, RJ, Brazil*  
E-mail: pavel@lenep.uenf.br

Received 14 September 2000; accepted June 2001

Two-phase flow in a porous medium can be modeled, using Darcy's law, in terms of the relative permeability functions of the two fluids (say, oil and water). The relative permeabilities generally depend not only on the fluid saturations but also on the direction in which the saturations are changing. During water injection, for example, the relative oil permeability  $k_{rO}$  falls gradually until a threshold is reached, at which stage the  $k_{rO}$  begins to decrease sharply. The latter stage is termed imbibition. If oil is subsequently injected, then  $k_{rO}$  does not recover along the imbibition path, but rather increases only gradually until another threshold is reached, whereupon it rises sharply. This second stage is called drainage, and the type of flow that occurs between the imbibition and drainage stages is called scanning flow. Changes in permeability during scanning flow are approximately reversible, whereas changes during drainage and imbibition are irreversible. Thus there is hysteresis, or memory, exhibited by the two-phase flow in the porous medium. In this work, we describe two models of permeability hysteresis. Common to both models is that the scanning flow regime is modeled with a family of curves along which the flow is reversible. In the Scanning Hysteresis Model (SHM), the scanning curves are bounded by two curves, the drainage and imbibition curves, where the flow can only occur in a specific direction. The SHM is a heuristic model consistent with experiments, but it does not have a nice mathematical specification. For instance, the algorithm for constructing solutions of Riemann problems involves several *ad hoc* assumptions. The Scanning Hysteresis Model with Relaxation (SHMR) augments the SHM by (a) allowing the scanning flow to extend beyond the drainage and imbibition curves and (b) treating these two curves merely as attractors of states outside the scanning region. The attraction, or relaxation, occurs on a time scale that corresponds to the redistribution of phases within the pores of the medium driven by capillary forces. By means of a formal Chapman–Enskog expansion, we show that the SHM with additional viscosity arises from the SHMR in the limit of vanishing relaxation time, provided that the diffusion associated with capillarity exceeds that induced by relaxation. Moreover, through a rigorous study of traveling waves in the SHMR, we show that the shock waves used to solve Riemann problems in the SHM are precisely those that have diffusive profiles. Thus the analysis of the SHMR justifies the SHM model. Simulations based on a simple numerical method for the simulation of flow with hysteresis confirm our analysis.

**Keywords:** drainage, imbibition, porous media flow, relative permeability hysteresis, scanning

## 1. Introduction

The flow properties of mixtures of oil and water in porous media are often modeled as if they depend only on the fraction of the fluid that is water, i.e., its saturation. However, one observes experimentally that this is not exactly true: it appears that the flow “remembers” its past history, in that it exhibits hysteresis in the fluid permeabilities. A natural explanation is that the distribution of the water and oil in the pores of different sizes plays a role in determining the local flow properties, and the distribution can change on a time scale that differs from that of the hydrodynamic waves in the flow.

In petroleum science, the hysteresis, or memory, effects observed in the experiments are usually described in a heuristic fashion. Therefore it is difficult to formulate well-defined mathematical models that take hysteresis into account. In this work, we propose a sound mathematical model of the hysteresis effects that involves relaxation of the permeability functions. We show that, in an appropriate limit, its solutions approach solutions of a simple heuristic model that is reasonably consistent with flow experiments. The proof involves analyzing traveling wave solutions of the relaxation model in the zero relaxation-time limit. When capillarity-induced diffusion is negligible, these waves are the admissible shock waves of the relaxation model, and we show that they coincide with the shock waves for the heuristic model. In particular, our results explain why the flow follows certain extreme paths when water saturation increases (the imbibition curve) or decreases (the drainage curve). We believe that our model is the first to provide a mathematical explanation for these experimentally well-established curves.

Hysteretic behavior in relative permeability has long been recognized [7,13]. Laboratory observations of permeability hysteresis for one-dimensional flow in cores, as well as physical explanations of the phenomena, have been presented by Owens and Archer [21], Colonna et al. [5], Gladfelter and Gupta [11], Morrow et al. [20], Kovscek et al. [15], and Braun and Holland [3]. Formulae for drainage, imbibition, and scanning relative permeability curves have been developed by Land [16], Killough [14], Aziz and Settari [1], Lenhard and Parker [17], and Guo [12]. The mathematical model for two-phase flow with hysteresis proposed by Marchesin et al. [19] considered two extreme fractional flow curves; scanning curves were not part of the model. A mathematical model for the fractional flow functions that does incorporate scanning curves was proposed by Furati [8–10]. The Riemann problem for this model was solved, and a classification of scale-invariant configurations was presented. Self-sharpening solutions were found for water flooding (described by a hyperbolic equation) and for polymer flooding (described by a system of two hyperbolic equations). One intriguing feature of this model is the existence of immobile saturation discontinuities.

An outline of the paper is as follows. In section 2 we review the physical modeling assumptions for two-phase flow in a porous medium. In section 3 we present a simple heuristic model (the SHM) of the hysteresis phenomena that are observed in experiments. We assume that the hysteretic relative permeability functions satisfy quali-

tative properties that hold in the experimental observations of Gladfelter and Gupta [11] and of Braun and Holland [3]. Solutions of Riemann problems for this model are reviewed in section 4. Then, in section 5, we introduce the SHMR, which is an extension of the SHM that includes relaxation. A formal Chapman–Enskog analysis of the SHMR, carried out in section 6, shows that its limit, as the relaxation time tends to zero, is the SHM augmented by a diffusion term. A rigorous analysis of traveling waves for the SHMR presented in section 7 determines precisely which shock waves have diffusive profiles. The SHMR also admits continuous stationary waves, which are constructed and analyzed in section 8. In section 9, we exemplify how to modify a numerical scheme to take hysteresis (as modeled in the SHM) into account. Numerical experiments comparing the SHM and the SHMR are presented in section 10; an application to cyclic water injection is also presented. Details of the specific permeability functions used throughout the paper are explained in appendix A.

## 2. Mathematical formulation of two-phase flow in porous media

Throughout this paper, the indices w and o refer to the water and oleic phases, respectively. In one spatial dimension, the flow is described by state quantities depending on  $(x, t)$ , the space and time coordinates. Principally, the state is determined by the fluid saturations, i.e., the fractions of the porous volume occupied by the phases, but it also depends on the distribution of the fluid in the pores, which might be described by auxiliary state variables. (In our model, such a state variable is the hysteresis parameter  $\pi$ .)

For phase  $l = w, o$ ,  $s_l$  is the saturation,  $\rho_l$  is the mass density (which we take to be constant),  $v_l$  is the seepage velocity (the product of the saturation and the particle velocity), and  $\mu_l$  is the viscosity. Since the fluids occupy the whole pore space,  $s_w + s_o = 1$ . Consequently, we may choose either  $s_w$  or  $s_o$  to determine both saturations.

The relative permeability of phase  $l$ , denoted by  $k_l$ , is a dimensionless function of saturation  $s_l$  measured in the laboratory;  $Kk_l$  is the capability of the porous medium to allow the flow of phase  $l$ , where  $K$  is the absolute permeability of the rock, which measures its capability of allowing the flow of a pure fluid. Another property of the rock is the porosity  $\phi$ , i.e., the fraction of the total volume occupied by pores. We take both  $K$  and  $\phi$  to be constant.

The capillary pressure is

$$p_c = p_o - p_w, \quad (2.1)$$

where  $p_w$  and  $p_o$  are the pressures in the water and the oil, respectively. The capillary pressure is found empirically to be a decreasing function of  $s_w$  [1]. Throughout this paper we neglect another type of hysteresis, capillary hysteresis, which is important in other flow regimes.

The conservation of water mass is

$$\frac{\partial}{\partial t}(\phi\rho_w s_w) + \frac{\partial}{\partial x}(\rho_w v_w) = 0, \quad (2.2)$$

where the first term represents accumulation of water mass and the second term represents transport of water mass. Similarly, the conservation of oil mass is

$$\frac{\partial}{\partial t}(\phi\rho_0s_0) + \frac{\partial}{\partial x}(\rho_0v_0) = 0. \quad (2.3)$$

According to an extension of Darcy's force law for two-phase flow in a porous medium, which is accurate for many flow regimes relevant to petroleum engineering, the seepage velocity of phase  $l$  is given by

$$v_l = -K \frac{k_l}{\mu_l} \frac{\partial p_l}{\partial x} \quad \text{for } l = w, o. \quad (2.4)$$

The total velocity is defined to be  $v = v_o + v_w$ . Dividing equations (2.2) and (2.3) by  $\rho_w$  and  $\rho_o$ , respectively, adding the results, and using  $s_w + s_o = 1$ , we obtain that

$$\frac{\partial v}{\partial x} = 0. \quad (2.5)$$

Thus  $v$  is a function solely of  $t$  and is determined by the boundary conditions. For simplicity, we take it to be nonzero and independent of time.

The water and oil fractional flow functions are defined, respectively, by

$$f_w = \frac{k_w/\mu_w}{k_w/\mu_w + k_o/\mu_o} \quad \text{and} \quad f_o = \frac{k_o/\mu_o}{k_w/\mu_w + k_o/\mu_o}. \quad (2.6)$$

It is easy to see that

$$vf_w = -K \frac{k_w}{\mu_w} \left( f_w \frac{\partial p_w}{\partial x} + f_o \frac{\partial p_o}{\partial x} \right) \quad (2.7)$$

and, using equation (2.1) and  $f_w + f_o = 1$ , that

$$vf_w = v_w - K \frac{k_w}{\mu_w} f_o \frac{\partial}{\partial x} p_c. \quad (2.8)$$

Substituting  $v_w$  from equation (2.8) into equation (2.2), we obtain the convection-diffusion equation

$$\frac{\partial}{\partial t}(\phi s_w) + \frac{\partial}{\partial x}(vf_w) = \frac{\partial}{\partial x} \left[ \varepsilon \frac{\partial}{\partial x} s_w \right], \quad (2.9)$$

where

$$\varepsilon = -K \frac{k_w}{\mu_w} f_o \frac{dp_c}{ds_w} \quad (2.10)$$

is the capillarity-induced diffusion coefficient. (This coefficient is sometimes taken, for simplicity, to be a small positive constant.) For  $v$  nonzero, we can set

$$t = \frac{\phi K}{v^2} \tilde{t} \quad \text{and} \quad x = \frac{K}{v} \tilde{x}, \quad (2.11)$$

thereby removing  $v$ ,  $\phi$ , and  $K$  from equations (2.9) and (2.10). For simplicity, we drop the tildes.

### 3. The Scanning Hysteresis Model

In this section, we describe a simplified version of the hysteresis phenomenon observed in the laboratory. This description gives rise to what we call the Scanning Hysteresis Model (SHM). This model for hysteresis in two-phase flow in a porous medium is based on a modified version of Darcy's law. For concreteness, we assume that the oil phase exhibits hysteresis, but the water phase does not. (This feature was observed in the experiments made by Gladfelter and Gupta [11] and by Braun and Holland [3].)

#### 3.1. Darcy's law in two-phase flow with hysteresis

Assume that a certain infinitesimal volume of the reservoir at position  $x$  and time  $t$  has oil saturation  $s_o(x, t)$  and water saturation  $s_w(x, t) = 1 - s_o(x, t)$ , and that the internal distribution of the two fluids in this volume, resulting from its past evolution, is characterized by the value of a parameter  $\pi(x, t)$ , which is called the hysteresis parameter. Using  $\pi$ , the SHM captures some of the complex behavior caused by hysteresis effects.

As the water permeability does not display hysteresis, it depends on the water saturation  $s_w$  but not on the hysteresis parameter  $\pi$ . See figure 1(a) for a typical graph of the water permeability  $k_w$  plotted vs.  $s := s_w$ . In contrast, the oil permeability

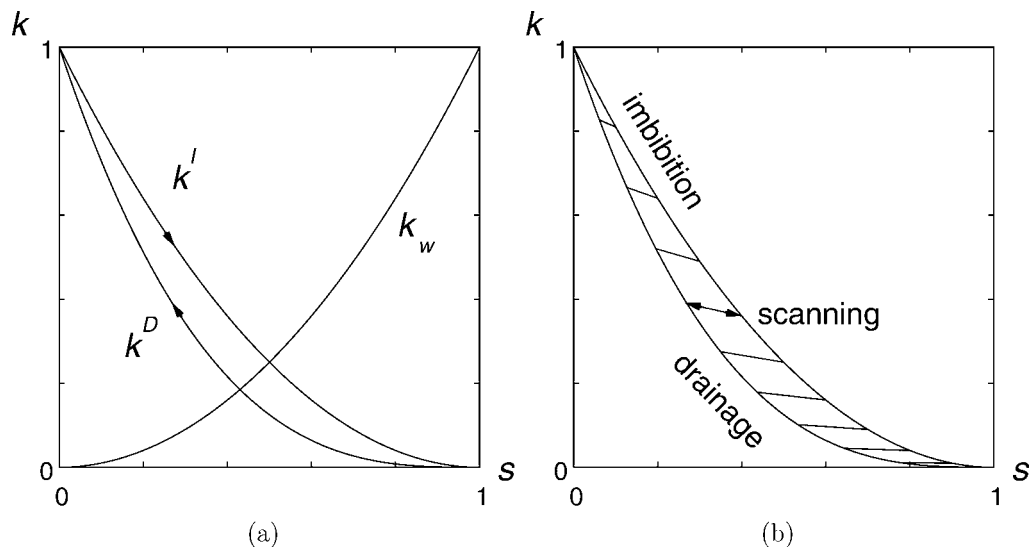


Figure 1. (a) Oil imbibition and drainage permeabilities  $k^I$  and  $k^D$  and water permeability  $k_w$  plotted vs.  $s := s_w$ . (b) Scanning curves for oil permeability (i.e., curves of constant  $\pi$ ).

depends not only on the fluid saturation but also on the hysteresis parameter and (in certain situations) on the saturation tendency.

First, consider the circumstance that the mixture of fluids is in a “scanning”, or reversible, state, which is defined by the range of oil saturations  $s_o^I(\pi) < s_o < s_o^D(\pi)$ . (The functions  $s_o^I(\pi)$  and  $s_o^D(\pi)$  are discussed below.) In this case, the oil permeability  $k_o$  is a given function of  $s_o$  and  $\pi$ :

$$k_o = k_o^S(s_o, \pi) \quad \text{if } s_o^I(\pi) < s_o < s_o^D(\pi) \quad (\text{i.e., in scanning flow}). \quad (3.1)$$

If the saturation is changed, the value of  $\pi$  describing the fluid state stays fixed, and the oil permeability changes with saturation following the “scanning curve” determined by the initial configuration, as in figure 1(b).

Movement along the interior of a scanning curve is reversible. However, if the oil saturation is increased too much, the internal configuration of the fluid changes. This change takes place when the state reaches the intersection of the scanning curve with the left-most curve in figure 1(b). This intersection occurs when  $s_o = s_o^D(\pi)$ . As long as the oil saturation continues to increase in time, the oil permeability follows this left-most curve. Since water “drains” when the oil saturation increases, this curve is called the drainage permeability curve, denoted by  $k_o^D(s_o)$ . Thus we have

$$k_o = k_o^D(s_o) \quad \text{if } s_o = s_o^D(\pi) \text{ and } \frac{\partial s_o}{\partial t} > 0 \quad (\text{i.e., in drainage flow}). \quad (3.2)$$

During drainage, the hysteresis parameter  $\pi$  changes. From the foregoing discussion, it follows that this happens in such a way that

$$k_o^D(s_o) = k_o^S(s_o, \pi) \quad \text{along the drainage curve}. \quad (3.3)$$

Solving this equation for  $s_o$  in terms of  $\pi$  gives  $s_o = s_o^D(\pi)$ .

Similarly, if, after starting in a scanning state, the oil saturation is decreased too much, then the state reaches the intersection  $s_o = s_o^I(\pi)$  of the scanning curve with the rightmost curve in figure 1(b). As long as the oil saturation continues decreasing in time, the oil permeability follows this imbibition permeability curve  $k_o^I(s_o)$ :

$$k_o = k_o^I(s_o) \quad \text{if } s_o = s_o^I(\pi) \text{ and } \frac{\partial s_o}{\partial t} < 0 \quad (\text{i.e., in imbibition flow}). \quad (3.4)$$

We also have that

$$k_o^I(s_o) = k_o^S(s_o, \pi) \quad \text{along the imbibition curve}; \quad (3.5)$$

this equation can be solved to give  $s_o = s_o^I(\pi)$ .

Finally, when the fluid state is in drainage or imbibition flow and the saturation tendency reverses sign, the flow returns to scanning mode. Only at the end states ( $s_o = 0$  and  $s_o = 1$ ), where the drainage and imbibition oil permeability curves intersect, can the state change directly between imbibition and drainage upon reversal of the saturation tendency.

*Remark 3.1.* The foregoing description involves an idealization, namely that the scanning curves are exactly reversible. Experimentally, a certain degree of hysteresis is observed even in the scanning region, i.e., scanning flow is only approximately reversible [3,11]. Because our description involves only one family of scanning curves, this feature is being ignored. Accounting for it involves at least a second family of scanning curves.

### 3.2. Notation and assumptions

As the hysteresis parameter  $\pi$  serves merely to distinguish the scanning curves, its values are rather arbitrary. For definiteness, we label the scanning curves by values of  $\pi$  that vary monotonically from 0 to 1. We also choose the water saturation  $s := s_w$  (rather than the oil saturation) to represent the fluid saturation. In keeping with these choices, we make the following definitions for  $s \in [0, 1]$  and  $\pi \in [0, 1]$ :

$$s^I(\pi) = 1 - s_o^I(\pi), \tag{3.6}$$

$$s^D(\pi) = 1 - s_o^D(\pi), \tag{3.7}$$

$$k^D(s) = k_o^D(1 - s), \tag{3.8}$$

$$k^I(s) = k_o^I(1 - s), \tag{3.9}$$

$$k^S(s, \pi) = k_o^S(1 - s, \pi) \quad \text{if } s^D(\pi) \leq s \leq s^I(\pi). \tag{3.10}$$

We also define the scanning, drainage, and imbibition regions to be

$$\mathcal{S} = \{(s, \pi) \in (0, 1) \times (0, 1): s^D(\pi) < s < s^I(\pi)\}, \tag{3.11}$$

$$\mathcal{D} = \{(s, \pi) \in (0, 1) \times (0, 1): s < s^D(\pi)\}, \tag{3.12}$$

$$\mathcal{I} = \{(s, \pi) \in (0, 1) \times (0, 1): s > s^I(\pi)\}. \tag{3.13}$$

These regions are shown in figure 2(a). (As we will see, the drainage and imbibition regions are inaccessible in the SHM, but they play a role in the relaxation model discussed in section 5.)

We make the following assumptions concerning the various functions that define the model (cf. figures 1 and 2):

$$k_w, k^D, \text{ and } k^I \text{ are } C^2, \text{ strictly monotone, and convex on } [0, 1]; \quad k^S \text{ is } C^2 \text{ on } \overline{\mathcal{S}}; \tag{3.14}$$

$$k_w(0) = 0, \quad k_w(1) = 1, \quad k^D(1) = k^I(1) = 0, \quad \text{and} \quad k^D(0) = k^I(0) = 1; \tag{3.15}$$

$$\frac{dk_w}{ds}(0) = 0, \quad \frac{dk^D}{ds}(1) = 0, \quad \text{and} \quad \frac{dk^I}{ds}(1) = 0; \tag{3.16}$$

$$\frac{\partial k^S}{\partial s}(s, \pi) < 0 \quad \text{for } (s, \pi) \in \overline{\mathcal{S}} \setminus \{(0, 0), (1, 1)\}; \tag{3.17}$$

$$\frac{\partial k^S}{\partial \pi}(s, \pi) < 0 \quad \text{for } (s, \pi) \in \overline{\mathcal{S}} \setminus \{(0, 0), (1, 1)\}; \tag{3.18}$$

$$k^D(s) < k^I(s) \quad \text{for } s \in (0, 1); \tag{3.19}$$

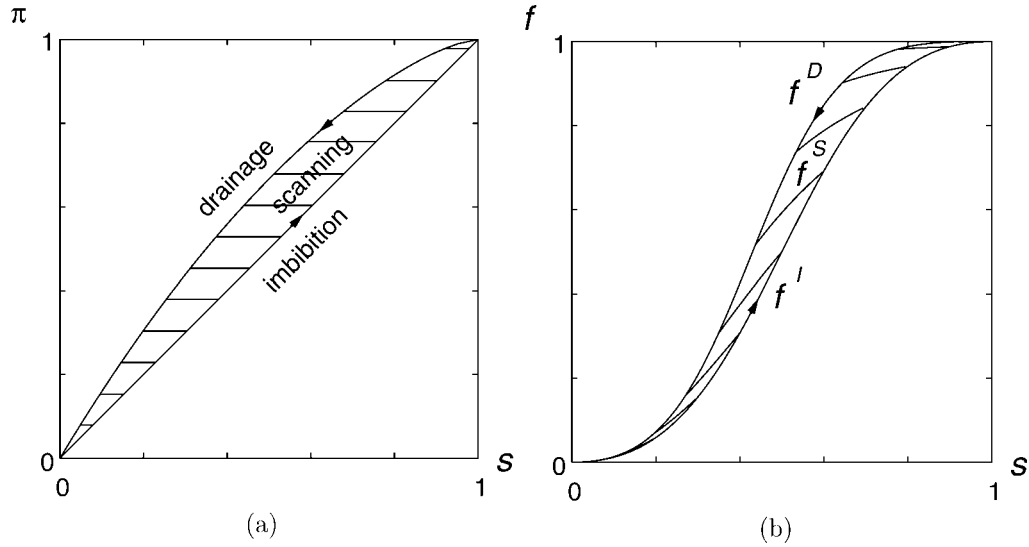


Figure 2. (a) The scanning, drainage, and imbibition regions in state space. (b) Fractional flow curves.

$$\frac{dk^D}{ds}(s) < \frac{\partial k^S}{\partial s}(s, \pi^D(s)) \quad \text{for } s \in (0, 1); \quad (3.20)$$

$$\frac{dk^I}{ds}(s) < \frac{\partial k^S}{\partial s}(s, \pi^I(s)) \quad \text{for } s \in (0, 1). \quad (3.21)$$

By assumptions (3.14) and (3.15) the water permeability increases as the water saturation does, whereas the oil permeability decreases as the water saturation increases along the drainage and imbibition curves. This assumption reflects the expectation that the flow of each fluid is impeded by the presence of the other. This expectation is also reflected in inequality (3.17), which says that the oil permeability decreases as the water saturation increases along any scanning curve. Inequality (3.18) guarantees that the scanning curves do not intersect. Inequality (3.19) holds, for example, in the experiments of Braun and Holland [3]. Inequalities (3.20) and (3.21) say that an oil scanning curve is less steep than the drainage (respectively, imbibition) curve at their intersection, so that these curves intersect transversely.

*Remark 3.2.* Models satisfying the opposite of inequality (3.17) have fundamentally different behavior and are not considered in this paper. The opposite of inequality (3.19) holds for some reservoir flows; we expect that it leads to results similar to those of the present paper.

Assumption (3.17) implies that the map taking  $(s, \pi) \in \mathcal{S}$  to  $(k, \pi) = (k^S(s, \pi), \pi)$  (from figure 2(a) to figure 1(b)) is an (orientation-reversing) invertible transformation. Assumptions (3.20) and (3.21) imply that  $s = s^D(\pi)$  and  $s = s^I(\pi)$  can be defined

implicitly by solving the equations

$$k^D(s^D(\pi)) = k(s^D(\pi), \pi) \quad \text{and} \quad k^I(s^I(\pi)) = k(s^I(\pi), \pi), \quad (3.22)$$

respectively. The functions  $s^D$  and  $s^I$  are increasing, as a consequence of the assumptions, and so have inverses, denoted by  $\pi = \pi^D(s)$  and  $\pi = \pi^I(s)$ , which are also increasing. (For the model shown in the figures,  $\pi^I(s) = s$ .) Later use will be made of the inequalities

$$\frac{d\pi^D}{ds} > 0 \quad \text{and} \quad \frac{d\pi^I}{ds} > 0. \quad (3.23)$$

### 3.3. The mathematical formulation of SHM

Following the manipulations and scalings explained in section 2, we obtain the Buckley–Leverett equation for  $s = s_w$ :

$$\frac{\partial s}{\partial t} + \frac{\partial}{\partial x} F(s, \pi) = \frac{\partial}{\partial x} \left( \varepsilon \frac{\partial s}{\partial x} \right). \quad (3.24)$$

Equation (3.24) is supplemented by the following definitions of the flux function  $F$  and equations for  $\pi$ , depending on where the state  $(s, \pi)$  lies and on the tendency of the saturation (see figure 2(a)):

$$F = f^D(s) := \frac{k_w(s)/\mu_w}{k_w(s)/\mu_w + k^D(s)/\mu_o} \quad \text{when } \pi = \pi^D(s) \text{ and } \frac{\partial s}{\partial t} < 0 \quad (3.25)$$

(drainage case);

$$F = f^I(s) := \frac{k_w(s)/\mu_w}{k_w(s)/\mu_w + k^I(s)/\mu_o} \quad \text{when } \pi = \pi^I(s) \text{ and } \frac{\partial s}{\partial t} > 0 \quad (3.26)$$

(imbibition case);

$$F = f^S(s, \pi) := \frac{k_w(s)/\mu_w}{k_w(s)/\mu_w + k^S(s, \pi)/\mu_o} \quad \text{and} \quad \frac{\partial \pi}{\partial t} = 0 \quad \text{otherwise} \quad (3.27)$$

(scanning case).

Notice that the scanning case occurs when either: (a)  $(s, \pi)$  lies in the scanning region  $\mathcal{S}$ ; (b)  $(s, \pi)$  lies on the drainage curve and  $\partial s/\partial t \geq 0$ ; or (c)  $(s, \pi)$  lies on the imbibition curve and  $\partial s/\partial t \leq 0$ . The fractional flow functions  $f^D$ ,  $f^I$ , and  $f^S$  are graphed in figure 2(b).

The equation  $\pi = \pi^D(s)$  that holds in the drainage case can be differentiated to relate  $\partial \pi/\partial t$  to  $\partial s/\partial t$ , which in turn can be expressed in terms of spatial derivatives using equation (3.24). This procedure yields an evolution equation for  $\pi$  in the drainage case. Similarly,  $\pi$  is governed by an evolution equation in the imbibition case. However, the resulting system of partial differential equations is fully nonlinear, not quasilinear, because the flux function depends on the sign of  $\partial s/\partial t$ . This dependence on the point values of  $\partial s/\partial t$  makes it difficult to define weak solutions of this system and to choose appropriate function spaces with which to analyze it.

#### 4. Solutions of Riemann problems for the SHM

In this section, we describe solutions of Riemann problems for the Scanning Hysteresis Model when capillary diffusion is negligible, i.e.,  $\varepsilon = 0$ . This assumption is the same as equating the fluid pressures in the water and in the oil. Solutions of Riemann problems were first derived in [2,8–10].

It follows from assumptions (3.14), (3.15) that:

- (i)  $f^D$  and  $f^I$  are zero at  $s = 0$  and equal to 1 at  $s = 1$ ;
- (ii) their derivatives are positive for  $s \in (0, 1)$  and vanish at  $s = 0$  and  $s = 1$ ; and
- (iii) that they each have at least one inflection point.

For simplicity in describing Riemann solutions, we assume that

$$f^D \text{ and } f^I \text{ each have a unique inflection point.} \quad (4.1)$$

When diffusion is neglected, the flow is governed by the following system of equations:

$$\frac{\partial s}{\partial t} + \frac{\partial}{\partial x} F(s, \pi) = 0, \quad (4.2)$$

$$\begin{cases} \pi = \pi^D(s) & \text{and } \frac{\partial s}{\partial t} < 0 & \text{(drainage),} \\ \text{or } \pi = \pi^I(s) & \text{and } \frac{\partial s}{\partial t} > 0 & \text{(imbibition),} \\ \text{or } \frac{\partial \pi}{\partial t} = 0 & \text{otherwise} & \text{(scanning),} \end{cases} \quad (4.3)$$

$$F(s, \pi) = \begin{cases} f^D(s) & \text{if } \pi = \pi^D(s) & \text{(drainage),} \\ f^I(s) & \text{if } \pi = \pi^I(s) & \text{(imbibition),} \\ f^S(s, \pi) & \text{if } \pi^I(s) < \pi < \pi^D(s) & \text{(scanning).} \end{cases} \quad (4.4)$$

A Riemann problem is an initial value-problem with discontinuous initial data:

$$(s, \pi)|_{t=0} = \begin{cases} (s_L, \pi_L) & \text{if } x < x_0, \\ (s_R, \pi_R) & \text{if } x > x_0. \end{cases} \quad (4.5)$$

As equations (4.2) and (4.3) are invariant under the scaling transformation  $(x, t) \mapsto (\alpha x, \alpha t)$  for  $\alpha > 0$ , Riemann solutions are taken to be scale-invariant, i.e., functions solely of  $x/t$ .

If the flow is in scanning mode the characteristic speeds of system (4.2)–(4.4) are  $a_s = \partial F / \partial s$  and  $a_0 = 0$ . In imbibition mode,

$$\frac{\partial \pi}{\partial t} + \frac{d\pi^I}{ds}(s) \frac{\partial}{\partial x} F(s, \pi) = 0, \quad (4.6)$$

so that the characteristic speeds are  $a_s = df^I/ds$  and  $a_0 = 0$ . Similarly, the characteristic speeds are  $a_s = df^D/ds$  and  $a_0 = 0$  in drainage mode. The waves associated to  $a_s$  are called saturation waves, and those associated to  $a_0$  are stationary, or standing, waves.

As the characteristic speed  $a_0$  is linearly degenerate, a scale-invariant stationary wave is discontinuous (i.e., it is a contact discontinuity). From equation (4.2) it follows that the states  $(s^-, \pi^-)$  and  $(s^+, \pi^+)$  on the left and right sides, respectively, of a stationary discontinuity must be related by the jump condition

$$F(s^-, \pi^-) = F(s^+, \pi^+). \tag{4.7}$$

Geometrically,  $(s^-, \pi^-)$  and  $(s^+, \pi^+)$  lie on the same horizontal line in the  $(s, f)$ -plane. Physically, such a stationary discontinuity represents an immobile discontinuity separating regions of the porous medium with differing histories (and therefore differing oil permeabilities).

A scale-invariant saturation wave is one of several varieties. If the flow is in scanning mode, with  $\pi$  fixed at some value  $\eta \in [0, 1]$ , it is simply a scale-invariant wave for the scalar conservation law (4.2). Such a wave is either a rarefaction wave, a shock wave, or a composite of rarefaction and (sonic) shock waves. In imbibition mode, the scalar conservation law

$$\frac{\partial s}{\partial t} + \frac{\partial}{\partial x} f^I(s) = 0 \tag{4.8}$$

is satisfied, so that a scale-invariant solution is either a rarefaction wave, a shock wave, or a composite of rarefaction and (sonic) shock waves for this equation. An analogous statement holds for waves in drainage mode.

Additionally, a scale-invariant saturation wave can involve a shock wave connecting a scanning state to an imbibition or drainage state. If the state on the left (respectively, right) side of the shock wave is denoted  $(s^-, \pi^-)$  (respectively,  $(s^+, \pi^+)$ ), then equation (4.2) requires the speed of the shock wave to be

$$\sigma = \frac{F(s^+, \pi^+) - F(s^-, \pi^-)}{s^+ - s^-}. \tag{4.9}$$

The authors of [2,8–10] assume that only certain shock waves correspond to physical solutions (as explained more fully below). In particular, the scanning state must be on the right side of the shock wave, and  $s^-$  must be greater than (respectively, less than)  $s^+$  in a scanning-to-imbibition (respectively, scanning-to-drainage) wave. A shock wave of one of these types can also be adjoined by rarefaction waves on either side to form a composite wave.

Stationary and saturation waves are used to solve Riemann problems. The construction of a Riemann solution is aided by the idea of an extended fractional flow func-

tion. Consider a fixed value  $\eta \in [0, 1]$  of the hysteresis parameter  $\pi$ . Following [6], we define the  $\eta$ -extended fractional flow function by

$$F^\eta(s) = \begin{cases} f^D(s) & \text{if } 0 \leq s \leq s^D(\eta), \\ f^S(s, \eta) & \text{if } s^D(\eta) < s < s^I(\eta), \\ f^I(s) & \text{if } s^I(\eta) \leq s \leq 1. \end{cases} \quad (4.10)$$

An example is shown in figure 3(a).

To solve the Riemann problem (4.5), we first take  $\eta = \pi_R$  and draw the  $\eta$ -extended fractional flow function  $F^\eta(s)$  in the  $(s, f)$ -plane. (See figure 3(b) for an example.) We identify the state  $(s_R, \pi_R)$  with the point  $R = (s_R, F^\eta(s_R))$  and the state  $(s_L, \pi_L)$  with the point  $L = (s_L, F(s_L, \pi_L))$ . Next we draw the horizontal straight line through  $L$ , and find its intersection with the graph of  $F^\eta$ ; this procedure defines the point  $M = (s_M, F^\eta(s_M))$ . (The intersection exists and is unique because  $F^\eta$  is an increasing function,  $F^\eta(0) = 0$ , and  $F^\eta(1) = 1$ .) The value of the hysteresis parameter for  $M$  depends on the segment of the graph of  $F^\eta$  to which the point  $M$  belongs:

$$\pi_M = \pi^D(s_M) \quad \text{if } 0 \leq s_M \leq s^D(\eta); \quad (4.11)$$

$$\pi_M = \eta = \pi_R \quad \text{if } s^D(\eta) \leq s_M \leq s^I(\eta); \quad (4.12)$$

$$\pi_M = \pi^I(s_M) \quad \text{if } s^I(\eta) \leq s_M \leq 1. \quad (4.13)$$

Because  $F(s_M, \pi_M) = F(s_L, \pi_L)$ , the state  $(s_M, \pi_M)$  is connected to  $(s_L, \pi_L)$  by a stationary discontinuity. Finally, we find the saturation wave connecting  $(s_M, \pi_M)$  to  $(s_R, \pi_R)$ . Such a wave has nonnegative speed, and therefore can appear to the right of

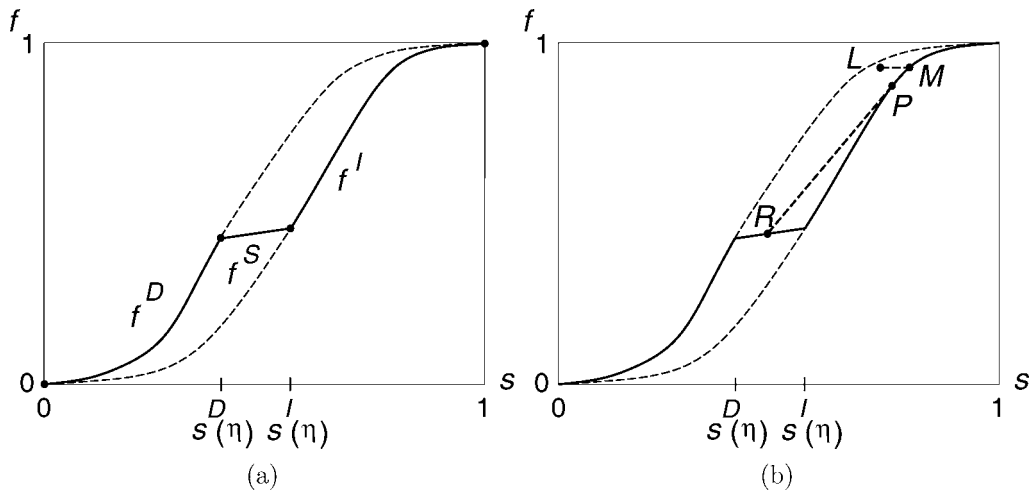


Figure 3. (a) The  $\eta$ -extended flow function  $F^\eta$  (solid curve). (b) An illustration of construction of a Riemann solution.

the stationary discontinuity. This wave is determined by solving the Riemann problem, with left state  $s_M$  and right state  $s_R$ , for the scalar conservation law

$$\frac{\partial s}{\partial t} + \frac{\partial}{\partial x} F^\eta(s) = 0. \tag{4.14}$$

The solution can be found using (a generalization of) Oleřnik’s convex envelope construction applied to the continuous, but only piecewise smooth, flux function  $F^\eta$ . For example, in figure 3(b), the saturation wave consists of an imbibition rarefaction wave from  $(s_M, \pi_M)$  to a point  $(s_P, \pi_P)$  adjoined, on its right side, by a scanning-to-imbibition shock wave from  $(s_P, \pi_P)$  to  $(s_R, \pi_R)$ . Once the saturation values within the saturation wave are known, the corresponding values for the hysteresis parameter are determined by requiring that  $F(s, \pi) = F^\eta(s)$ .

The Riemann solution therefore consists of the stationary wave connecting the state  $(s_L, \pi_L)$  to an intermediate state  $(s_M, \pi_M)$  and a saturation wave connecting the intermediate state to  $(s_R, \pi_R)$ .

*Remark 4.1.* In the SHM, there is a family of loop solutions associated with each state  $I$  on the imbibition curve, as illustrated in figure 4. Each solution consists of a sequence of three waves: a stationary discontinuity from  $L = I$  to a point  $M$  in the scanning region, a scanning wave group from  $M$  to another point  $P$  on the imbibition curve, and an imbibition wave group from  $P$  to  $R = I$ . In the  $(s, f)$ -plane, such a solution appears as a triangle with curved edges. Each loop solution is parametrized by a wave strength, which we may measure with the difference in saturation between the states  $M$  and  $P$ . (In  $(x, t)$ -plane, there are other free parameters needed to fully describe such solutions, such as the width occupied by each constant state  $M$  and  $P$ .) Analogously, there is a family of loop solutions associated with each state on the drainage curve.

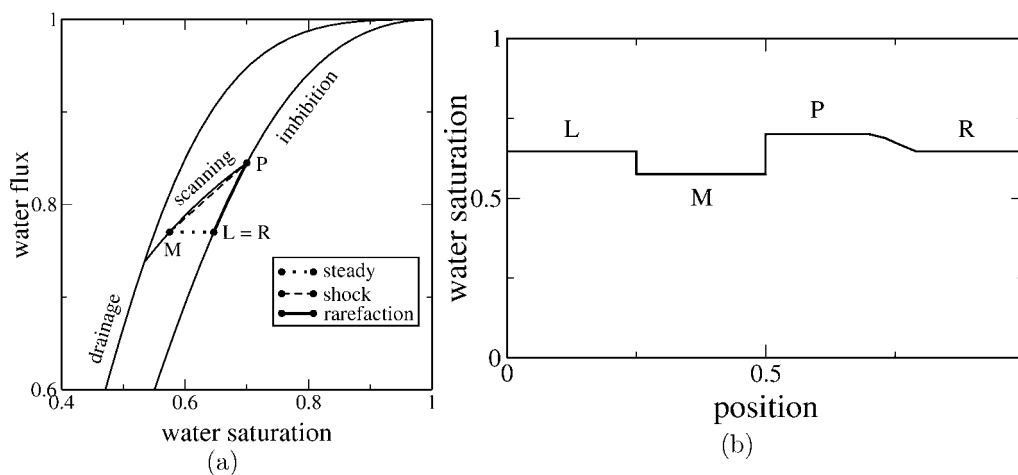


Figure 4. Loop solution.

Such loop solutions exist if the three waves are separated, since the speeds of the waves are distinct and ordered so that their separations increase with time. Because the left state and right state coincide, they are striking examples of multiple solutions for the Riemann problem, viewed as time-asymptotic solutions of the conservation laws: each such loop is also a solution for the Riemann problem with constant initial data  $L = R$ . For the same reason, it is often possible to insert such a loop in a Riemann solution and thereby obtain another solution.

## 5. The Scanning Hysteresis Model with relaxation

In this section, we introduce a model of hysteresis with (one-sided) relaxation and diffusion, the Scanning Hysteresis Model with Relaxation (SHMR). To motivate the addition of relaxation, consider a flow in which the water saturation  $s$  is increased to the critical imbibition saturation,  $s^I(\pi)$ , and continues increasing. In the SHM,  $\pi$  adjusts continuously during imbibition to maintain  $s = s^I(\pi)$ , meaning that the configuration of the water and oil in the pores is in equilibrium. In reality, the fluid configuration is perturbed from equilibrium by the increase in  $s$  and is driven back to equilibrium, in a short time, by capillary forces. Similar behavior occurs during drainage. Accordingly, in the SHMR, we allow the fluid state to be out of equilibrium, i.e.,  $s > s^I(\pi)$  or  $s < s^D(\pi)$ , and introduce dynamics for  $\pi$  so that it relaxes back to equilibrium on a time scale  $\tau$ .

*Remark 5.1.* Hysteresis in two-phase flow is analogous to the behavior of a ductile metal, which behaves elastically (reversibly) unless it is subjected to forces that exceed its yield stress, whereupon it deforms plastically (irreversibly). When strain rates are small, plasticity is described by a model that is rate-independent: the metal behaves plastically immediately upon reaching the yield stress (if the stress continues to increase). Such a model has a structure similar to the SHM. In contrast, a rate-dependent plasticity model (viscoplastic model) is required when strain rates are large. This type of model allows the instantaneous stress to exceed yield and introduces a time scale for relaxation of the stress toward the yield stress. The SHMR is analogous to, and was motivated by, rate-dependent models of plasticity.

To construct the SHMR, we first extend each scanning permeability curve (i.e.,  $k = k^S(s, \pi)$  for fixed  $\pi$ ) beyond the scanning interval  $s^D(\pi) \leq s \leq s^I(\pi)$  on which it is measured. For mathematical simplicity, we choose a  $C^2$  extension  $\hat{k}^S$  of  $k^S$  defined for all  $s \in [0, 1]$  and  $\pi \in [0, 1]$ . Of course, this extended function is not unique, but analysis of the model will show that solutions of the SHMR are affected by the choice of extension only in the vicinity of the drainage and imbibition curves. Associated to the extended scanning permeability function is the extended fractional flow function:

$$f(s, \pi) = \frac{k_w(s)/\mu_w}{k_w(s)/\mu_w + \hat{k}^S(s, \pi)/\mu_o}. \quad (5.1)$$

Secondly, we introduce a forcing term  $g(s, \pi)$  in the differential equation for  $\pi$ . We take  $g(s, \pi) = 0$  for  $(s, \pi) \in \mathcal{S}$ , so that  $\pi$  remains unchanged when the flow is in the scanning region. On the other hand, when the flow is outside the scanning region,  $g(s, \pi)$  drives  $\pi$  towards the imbibition and drainage curves, and this tendency grows with increasing deviation of  $\pi$  from equilibrium. As we will see, solutions of the SHMR are rather insensitive to the choice of the forcing function, so we take  $g(s, \pi)$  to have a particularly simple form.

The SHMR is defined by the following quasilinear system of partial differential equations:

$$\frac{\partial s}{\partial t} + \frac{\partial}{\partial x} f(s, \pi) = \frac{\partial}{\partial x} \left( \varepsilon \frac{\partial s}{\partial x} \right), \tag{5.2}$$

$$\frac{\partial \pi}{\partial t} = g(s, \pi) := \begin{cases} \frac{\pi^I(s) - \pi}{\tau} & \text{if } \pi < \pi^I(s), \\ \frac{\pi^D(s) - \pi}{\tau} & \text{if } \pi > \pi^D(s), \\ 0 & \text{otherwise.} \end{cases} \tag{5.3}$$

The constant  $\tau > 0$  is the relaxation time.

The vanishing relaxation introduced in (5.3) yields nice mathematical properties to the solution of the system, but we do not attribute to (5.3) any direct physical meaning.

*Remark 5.2.* We emphasize that the only role of the imbibition and drainage curves in the SHMR is to serve as attractors for external states. No flow orientation is associated *a priori* with these curves.

## 6. Formal analysis of the SHMR

In this section, we show that the scanning hysteresis model formally arises as the rate-independent limit ( $\tau \rightarrow 0^+$ ) of the Scanning Hysteresis Model with relaxation. To determine this limit, we proceed formally, following [18], using an expansion similar in spirit to the Chapman–Enskog expansion for Boltzmann equation [4].

Suppose that, in a certain region of the  $(x, t)$ -plane,  $s$  and  $\pi$  are smooth functions and that  $\pi \leq \pi^I(s)$ . Then

$$\tau \frac{\partial \pi}{\partial t} = \pi^I(s) - \pi. \tag{6.1}$$

In the limit  $\tau \rightarrow 0^+$ ,  $\pi$  tends to  $\pi^I(s)$ . Let us write the solution for  $\tau > 0$  in terms of an asymptotic expansion in  $\tau$ :

$$\pi = \pi^I(s) + \tau \pi_1 + O(\tau^2). \tag{6.2}$$

Then, because  $f^I(s) = f(s, \pi^I(s))$ , Taylor's theorem implies that

$$f(s, \pi) = f^I(s) + \tau \frac{\partial f}{\partial \pi}(s, \pi^I(s))\pi_1 + \mathcal{O}(\tau^2), \quad (6.3)$$

so that

$$\frac{\partial s}{\partial t} = -\frac{df^I}{ds}(s) \frac{\partial s}{\partial x} + \mathcal{O}(\tau). \quad (6.4)$$

Also, from equation (6.1), we find that

$$\tau \frac{\partial}{\partial t} [\pi^I(s) + \tau \pi_1 + \mathcal{O}(\tau^2)] = -\tau \pi_1 + \mathcal{O}(\tau^2), \quad (6.5)$$

so that

$$\pi_1 = -\frac{d\pi^I}{ds}(s) \frac{\partial s}{\partial t} + \mathcal{O}(\tau). \quad (6.6)$$

Therefore, by equations (6.3), (6.4), and (6.6),

$$f(s, \pi) = f^I(s) + \tau \frac{\partial f}{\partial \pi}(s, \pi^I(s)) \frac{d\pi^I}{ds}(s) \frac{df^I}{ds}(s) \frac{\partial s}{\partial x} + \mathcal{O}(\tau^2). \quad (6.7)$$

Implicit differentiation shows that

$$\frac{df^I}{ds}(s) = \frac{\partial f}{\partial s}(s, \pi^I(s)) + \frac{\partial f}{\partial \pi}(s, \pi^I(s)) \frac{d\pi^I}{ds}(s). \quad (6.8)$$

Equations (6.7) and (6.8) combine to give

$$f(s, \pi) = f^I(s) + \tau \left[ \frac{df^I}{ds}(s) - \frac{\partial f}{\partial s}(s, \pi^I(s)) \right] \frac{df^I}{ds}(s) \frac{\partial s}{\partial x} + \mathcal{O}(\tau^2). \quad (6.9)$$

Therefore

$$\frac{\partial s}{\partial t} + \frac{\partial}{\partial x} f^I(s) = \frac{\partial}{\partial x} \left[ (\varepsilon - \nu^I) \frac{\partial s}{\partial x} \right] + \mathcal{O}(\tau^2), \quad (6.10)$$

where

$$\nu^I = \tau \left[ \frac{df^I}{ds}(s) - \frac{\partial f}{\partial s}(s, \pi^I(s)) \right] \frac{df^I}{ds}(s). \quad (6.11)$$

Additionally, the assumption that  $\pi \leq \pi^I(s)$  entails that  $\pi_1 \leq 0$ , i.e., as  $d\pi^I/ds > 0$  in equation (6.6),

$$\frac{\partial s}{\partial t} \geq 0. \quad (6.12)$$

Thus we find that, in the  $\tau \rightarrow 0^+$  limit of equations (6.10) and (6.1), a smooth solution formally satisfies

$$\frac{\partial s}{\partial t} + \frac{\partial}{\partial x} f^I(s) = \frac{\partial}{\partial x} \left[ (\varepsilon - \nu^I) \frac{\partial s}{\partial x} \right] \quad (6.13)$$

when

$$\pi = \pi^I(s), \quad \frac{\partial s}{\partial t} \geq 0. \tag{6.14}$$

Similarly, it satisfies

$$\frac{\partial s}{\partial t} + \frac{\partial}{\partial x} f^D(s) = \frac{\partial}{\partial x} \left[ (\varepsilon - \nu^D) \frac{\partial s}{\partial x} \right], \tag{6.15}$$

where

$$\nu^D = \tau \left[ \frac{df^D}{ds}(s) - \frac{\partial f}{\partial s}(s, \pi^D(s)) \right] \frac{df^D}{ds}(s), \tag{6.16}$$

when

$$\pi = \pi^D(s) \quad \text{and} \quad \frac{\partial s}{\partial t} \leq 0. \tag{6.17}$$

Finally, in a region of the  $(x, t)$ -plane where  $s$  and  $\pi$  are smooth and  $\pi^I(s) < \pi < \pi^D(s)$ , the  $\tau \rightarrow 0^+$  limit satisfies

$$\frac{\partial s}{\partial t} + \frac{\partial}{\partial x} f(s, \pi) = \frac{\partial}{\partial x} \left( \varepsilon \frac{\partial s}{\partial x} \right), \tag{6.18}$$

$$\frac{\partial \pi}{\partial t} = 0. \tag{6.19}$$

*Remark 6.1.* Note that this analysis suggests that  $\tau$  should be small enough to ensure  $\varepsilon > \nu^I$  and  $\varepsilon > \nu^D$  in order to have a positive diffusion coefficient. This feature is discussed further in remark 7.9.

### 7. Traveling waves in the SHMR

The SHMR also admits traveling wave solutions that tend, as  $\tau \rightarrow 0^+$ , to discontinuous solutions of the SHM. For this kind of solution,  $s$  and  $\pi$  depend only on the variable  $\xi = x - \sigma t$ , where the constant  $\sigma$  is the speed of propagation. The solution tends to the states  $(s^-, \pi^-)$  and  $(s^+, \pi^+)$  as  $\xi \rightarrow -\infty$  and  $\xi \rightarrow +\infty$ , respectively.

Inserting this form of solution into equations (5.2) and (5.3), we obtain that

$$\begin{cases} -\sigma s_\xi + f(s, \pi)_\xi = (\varepsilon s_\xi)_\xi, \\ -\sigma \pi_\xi = g(s, \pi). \end{cases} \tag{7.1}$$

Integrating the first equation from  $\xi = -\infty$  yields

$$\begin{cases} \varepsilon s_\xi = -\sigma (s - s^-) + f(s, \pi) - f(s^-, \pi^-), \\ -\sigma \pi_\xi = g(s, \pi), \end{cases} \tag{7.2}$$

which is a system of ordinary differential equations for  $s$  and  $\pi$ , with  $\xi$  playing the role of “time.” In the following we will use the notation  $(\dot{s}, \dot{\pi})$  for  $(s_\xi, \pi_\xi)$ .

### 7.1. Character of the equilibria

The states  $(s^-, \pi^-)$  and  $(s^+, \pi^+)$  must be equilibria for system (7.2). If  $s^- \neq s^+$ , then a necessary condition for  $(s^-, \pi^-)$  to be connected by a traveling wave to  $(s^+, \pi^+)$  is that

$$\sigma = \frac{f(s^+, \pi^+) - f(s^-, \pi^-)}{s^+ - s^-}, \quad (7.3)$$

$$g(s^-, \pi^-) = 0, \quad g(s^+, \pi^+) = 0. \quad (7.4)$$

On the other hand, if  $s := s^- = s^+$ , then  $f(s, \pi^-)$  must equal  $f(s, \pi^+)$ ; by equation (5.1),  $\hat{k}^S(s, \pi^-) = \hat{k}^S(s, \pi^+)$ , and assumption (3.18) implies that  $\pi^- = \pi^+$ , meaning that there is no discontinuity.

In the following discussion, we will often treat  $(s^-, \pi^-)$  as fixed, and it proves useful to define

$$h(s, \pi; s^-, \pi^-, \sigma) = -\sigma(s - s^-) + f(s, \pi) - f(s^-, \pi^-), \quad (7.5)$$

which we will sometimes denote simply as  $h(s, \pi)$ .

**Lemma 7.1.** A state  $(s^e, \pi^e)$  is an equilibrium for system (7.2) if and only if  $(s^e, \pi^e)$  is a scanning, imbibition, or drainage state with  $h(s^e, \pi^e) = 0$ . In other words,  $(s^e, \pi^e) \in \overline{S}$  and the corresponding point  $(s^e, f(s^e, \pi^e))$  lies on the line with slope  $\sigma$  drawn through  $(s^-, f(s^-, \pi^-))$  in the  $(s, f)$ -plane.

*Proof.* Since  $(s^e, \pi^e)$  is an equilibrium, the first equation in system (7.2) requires that  $h(s^e, \pi^e; s^-, \pi^-, \sigma) = 0$ . The second equation in system (7.2) requires that  $g(s^e, \pi^e) = 0$ . But  $g(s^e, \pi^e) > 0$  unless  $(s^e, \pi^e)$  is a scanning, drainage or imbibition state.  $\square$

The local flow near an equilibrium is described in the following lemma. Notice that, when an equilibrium point lies on the imbibition curve, the local flow in the imbibition region, where  $g(s, \pi) = [\pi^1(s) - \pi]/\tau$ , differs from the behavior in the scanning region, where  $g$  vanishes, and analogously for an equilibrium on the drainage curve.

**Lemma 7.2.** Consider an equilibrium point  $(s^e, \pi^e)$  for system (7.2). Assuming that  $\tau > 0$  is sufficiently small, the following statements hold.

- (i) If  $(s^e, \pi^e)$  lies strictly inside the scanning region, then the scanning curve  $\pi = \pi^e$  contains the only orbit of system (7.2) through  $(s^e, \pi^e)$ . Moreover,  $(s^e, \pi^e)$  is an attractor (respectively, repeller) if and only if  $(\partial f/\partial s)(s^e, \pi^e) - \sigma$  is negative (respectively, positive).
- (ii) If  $(s^e, \pi^e)$  lies on the imbibition curve, then:
  - (a) in the scanning region, the flow is as in (i);

- (b) in the imbibition region, the linearization of system (7.2) has one positive eigenvalue and one eigenvalue of the same sign as  $(df^I/ds)(s^e) - \sigma$ . The latter has the smaller absolute value, so we refer to it as the weak eigenvalue. The corresponding eigenvectors are, respectively,

$$\begin{pmatrix} O(\tau) \\ 1 \end{pmatrix} \quad \text{and} \quad \begin{pmatrix} 1 - \frac{\sigma\tau}{\varepsilon} \left[ \frac{df^I}{ds}(s^e) - \sigma \right] + O(\tau^2) \\ \frac{d\pi^I}{ds}(s^e) \end{pmatrix}. \quad (7.6)$$

(iii) If  $(s^e, \pi^e)$  lies on the drainage curve, then a statement analogous to (ii) holds.

*Proof.* First, suppose that  $(s^e, \pi^e)$  is an equilibrium lying strictly inside the scanning region ( $s^D(\pi^e) < s^e < s^I(\pi^e)$ ). Then, as  $g = 0$  throughout the scanning region,  $\dot{\pi}$  must vanish along any orbit through  $(s^e, \pi^e)$ . Thus such an orbit is contained in the scanning curve  $\pi = \pi^e$ . Along this curve, the dynamics is determined by the first equation of system (7.2). In particular, by differentiating  $h$  with respect to  $s$ , we see that  $s^e$  is an attractor (respectively, repeller) according as  $(\partial f/\partial s)(s^e, \pi^e) - \sigma$  is negative (respectively, positive).

Second, consider an equilibrium  $(s^e, \pi^e)$  on the imbibition curve. According to the formula for  $g$  in equation (5.3), the linearization of system (7.2) in the imbibition region  $\pi < \pi^I(s)$  has matrix

$$A^e = \begin{pmatrix} \frac{1}{\varepsilon} \left[ \frac{\partial f}{\partial s}(s^e, \pi^e) - \sigma \right] & \frac{1}{\varepsilon} \frac{\partial f}{\partial \pi}(s^e, \pi^e) \\ -\frac{1}{\sigma\tau} \frac{d\pi^I}{ds}(s^e) & \frac{1}{\sigma\tau} \end{pmatrix}. \quad (7.7)$$

Therefore

$$\text{tr } A^e = \frac{1}{\varepsilon} \left[ \frac{\partial f}{\partial s}(s^e, \pi^e) - \sigma \right] + \frac{1}{\sigma\tau} \quad (7.8)$$

and, since  $f^I(s) = f(s, \pi^I(s))$ ,

$$\det A^e = \frac{1}{\varepsilon\sigma\tau} \left[ \frac{\partial f}{\partial s}(s^e, \pi^e) - \sigma + \frac{\partial f}{\partial \pi}(s^e, \pi^e) \frac{d\pi^I}{ds}(s^e) \right] = \frac{1}{\varepsilon\sigma\tau} \left[ \frac{df^I}{ds}(s^e) - \sigma \right]. \quad (7.9)$$

Notice that, if  $\tau$  is sufficiently small, then both the trace and the discriminant of  $A^e$  (*viz.*,  $(\text{tr } A^e)^2 - 4\det A^e$ ) are positive. Thus, in the imbibition region, the equilibrium  $(s^e, \pi^e)$  is a repelling node when  $(df^I/ds)(s^e) > \sigma$  and a saddle point when  $(df^I/ds)(s^e) < \sigma$ .

In fact, for small  $\tau$ , the eigenvalues of  $A^e$  are

$$\frac{1}{2} \text{tr } A^e \left\{ 1 \pm \sqrt{1 - \frac{4(\det A^e)}{(\text{tr } A^e)^2}} \right\} = \begin{cases} \frac{1}{\sigma\tau} + O(1), \\ \frac{1}{\varepsilon} \left[ \frac{df^I}{ds}(s^e) - \sigma \right] + O(\tau), \end{cases} \quad (7.10)$$

and the corresponding eigenvectors are as in equation (7.6). □

7.2. Barrier curve

In this subsection, we construct a curve  $\Gamma_\tau^I$  in the  $(s, \pi)$ -plane called a barrier curve. This curve crosses the imbibition curve precisely at equilibria, and it approaches the imbibition curve as  $\tau \rightarrow 0^+$ . It is a graph  $\pi = \pi_\tau^I(s)$  over an interval  $s \in [s_{\tau, \min}^I, s_{\tau, \max}^I]$ , where  $s_{\tau, \min}^I \rightarrow 0$  and  $s_{\tau, \max}^I \rightarrow 1$  as  $\tau \rightarrow 0^+$ . Moreover, at each point on the barrier curve, the vector  $(\dot{s}, \dot{\pi})$  defined by system (7.2) is oriented so that orbits are trapped between the barrier curve and the imbibition curve. These features are illustrated, for a particular case, in figure 5. A barrier curve  $\Gamma_\tau^D$  related to the drainage curve can be constructed analogously, but we omit the details. Barrier curves facilitate the proofs in section 7.3.

**Lemma 7.3.** Assume that  $(s^-, \pi^-)$  lies on the imbibition curve and that  $\sigma > 0$ . Fix  $b > 1$  and consider the barrier curve  $\Gamma_\tau^I$  in the  $(s, \pi)$ -plane defined implicitly by the equation

$$\pi = \pi^I(s) + \frac{\sigma \tau b}{\varepsilon} \frac{d\pi^I}{ds}(s) h(s, \pi; s^-, \pi^-, \sigma). \tag{7.11}$$

Then, for all sufficiently small  $\tau \geq 0$ :

- (i)  $\Gamma_\tau^I$  is a smooth graph  $\pi = \pi_\tau^I(s)$ ,  $s \in [s_{\tau, \min}^I, s_{\tau, \max}^I]$ , that reduces to the imbibition curve  $\pi = \pi^I(s)$ ,  $s \in [0, 1]$ , when  $\tau = 0$ ;
- (ii) for  $\tau > 0$ , the barrier curve intersects the imbibition curve at the point  $(s, \pi_\tau^I(s)) = (s, \pi^I(s))$  if and only if

$$\sigma(s - s^-) = f^I(s) - f^I(s^-), \tag{7.12}$$

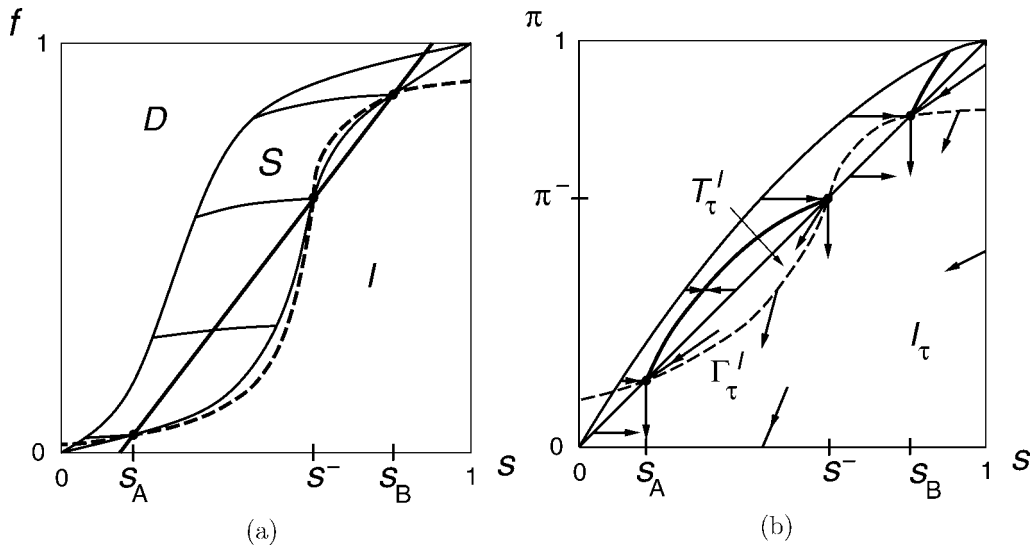


Figure 5. Barrier curve (dashed) for a particular case.

so that, if  $s \neq s^-$ ,  $\sigma$  is the slope of the chord joining  $(s^-, f^I(s^-))$  to  $(s, f^I(s))$ ; such intersection points are the equilibria of system (7.2) lying on the imbibition curve;

- (iii) similarly, the point  $(s, \pi_\tau^I(s))$  on the barrier curve lies in the imbibition region if and only if

$$\sigma(s - s^-) > f^I(s) - f^I(s^-), \tag{7.13}$$

and it lies in the scanning region if and only if

$$\sigma(s - s^-) < f^I(s) - f^I(s^-); \tag{7.14}$$

- (iv) at a barrier point lying in the imbibition region  $\mathcal{I}$ , the vector  $(\dot{s}, \dot{\pi})$  defined by system (7.2) points into the region

$$\mathcal{I}_\tau = \{(s, \pi) \in \mathcal{I}: \pi < \pi_\tau^I(s) \text{ if } s \in (s_{\tau, \min}^I, s_{\tau, \max}^I)\}; \tag{7.15}$$

- (v) at a barrier point lying on the imbibition curve, the slope of the weak eigenvector lies between the slopes of the barrier and imbibition curves.

*Proof.* Setting  $\tau = 0$  in equation (7.11) shows that  $\Gamma_0^I$  is the imbibition curve for  $\tau > 0$ , and application of the Implicit Function Theorem to solve equation (7.11) for  $\pi$  in terms of  $s$  and  $\tau$  yields statement (i). If  $\tau \neq 0$ , then as  $d\pi^I/ds > 0$ , a point  $(s, \pi)$  on  $\Gamma_\tau^I$  lies on the imbibition curve if and only if  $h = 0$  at this point, i.e., equation (7.12) holds. Implicit differentiation shows that, at a point  $(s, \pi)$  on  $\Gamma_0^I$ ,

$$\left. \frac{\partial \pi_\tau^I}{\partial \tau} \right|_{\tau=0} = \frac{\sigma b}{\varepsilon} \frac{d\pi^I}{ds} h. \tag{7.16}$$

This quantity is negative, and therefore  $\Gamma_\tau^I$  lies below the imbibition curve for  $\tau > 0$ , if and only if  $(s - s^-)\sigma > f^I(s) - f^I(s^-)$ .

According to equations (7.2), (5.3), and (7.11), the vector field at a point  $(s, \pi)$  on  $\Gamma_\tau^I$  inside the imbibition region is

$$\dot{s} = \frac{h}{\varepsilon} < 0, \tag{7.17}$$

$$\dot{\pi} = \frac{\pi^I(s) - \pi}{-\sigma \tau} = \frac{b}{\varepsilon} \frac{d\pi^I}{ds} h < 0. \tag{7.18}$$

Thus the slope of the vector  $(\dot{s}, \dot{\pi})$  is  $b d\pi^I/ds$ , which exceeds the slope  $d\pi^I/ds + O(\tau)$  of  $\Gamma_\tau^I$  because  $b > 1$ . This establishes statement (iv).

At a barrier point  $(s, \pi)$  lying on the imbibition curve,  $h = 0$  by equation (7.12). Therefore the slope of  $\Gamma_\tau^I$  is determined by implicit differentiation of equation (7.11):

$$\frac{d\pi_\tau^I}{ds} = \frac{d\pi^I}{ds} \left[ 1 + \frac{\sigma \tau b}{\varepsilon} \left( \frac{\partial f}{\partial s} - \sigma \right) \right] + \frac{\sigma \tau b}{\varepsilon} \frac{d\pi^I}{ds} \frac{\partial f}{\partial \pi} \frac{d\pi_\tau^I}{ds}. \tag{7.19}$$

Since

$$\frac{df^I}{ds} = \frac{\partial f}{\partial s} + \frac{d\pi^I}{ds} \frac{\partial f}{\partial \pi}, \quad (7.20)$$

$$\frac{d\pi^I}{ds} = \frac{1 + \frac{\sigma\tau b}{\varepsilon} \left( \frac{df^I}{ds} - \sigma - \frac{d\pi^I}{ds} \frac{\partial f}{\partial \pi} \right)}{1 - \frac{\sigma\tau b}{\varepsilon} \frac{d\pi^I}{ds} \frac{\partial f}{\partial \pi}} \frac{d\pi^I}{ds} = \left[ 1 + \frac{\sigma\tau b}{\varepsilon} \left( \frac{df^I}{ds} - \sigma \right) [1 + O(\tau)] \right] \frac{d\pi^I}{ds}. \quad (7.21)$$

On the other hand, the slope of the weak eigenvector, given by the second of equations (7.6), is

$$\left[ 1 + \frac{\sigma\tau}{\varepsilon} \left( \frac{df^I}{ds} - \sigma \right) [1 + O(\tau)] \right] \frac{d\pi^I}{ds}, \quad (7.22)$$

and the slope of the imbibition curve is  $d\pi^I/ds$ . Recalling that  $b > 1$  yields statement (v).  $\square$

In particular, this result associates a curve  $\Gamma_\tau^I$  and a region  $\mathcal{I}_\tau$  to an imbibition point  $(s^-, \pi^-)$ , a speed  $\sigma > 0$ , and a choice of  $b > 1$ . For  $\tau > 0$ , a point  $(s, \pi)$  on the boundary of the region  $\mathcal{I}_\tau$  is one of the following types:

- (i) a point on the imbibition curve  $\pi = \pi^I(s)$  such that  $\sigma(s - s^-) \leq f^I(s) - f^I(s^-)$ ;
- (ii) a point on the barrier curve  $\pi = \pi^I(s)$  such that  $\sigma(s - s^-) \geq f^I(s) - f^I(s^-)$ ;
- (iii) a point on the bottom boundary  $\pi = 0$  such that  $s \in [s_{\tau, \min}^I, 1]$ ; or
- (iv) a point on the right side boundary  $s = 1$  such that  $\pi \in [0, \pi_\tau^I(s_{\tau, \max}^I)]$ .

The corresponding vector  $(\dot{s}, \dot{\pi})$  for each of the foregoing types of points on  $\partial\mathcal{I}_\tau$  satisfies: (i)  $\dot{s} \geq 0$  and  $\dot{\pi} = 0$ ; (ii)  $(\dot{s}, \dot{\pi})$  points into  $\mathcal{I}_\tau$ ; (iii)  $\dot{\pi} \leq 0$ ; or (iv)  $\dot{s} \leq 0$ . These facts are illustrated in figure 5(b). Therefore an orbit that lies in  $\overline{\mathcal{I}_\tau}$  at  $\xi = \xi_0$  must remain in  $\overline{\mathcal{I}_\tau}$  for  $\xi > \xi_0$ . (However, such an orbit might arrive at the bottom boundary  $\pi = 0$  within a finite interval in  $\xi$ .) In fact, it cannot approach an equilibrium of system (7.2) as  $\xi \rightarrow \infty$  unless it starts at an equilibrium at  $\xi = \xi_0$ .

Similarly, if we define the imbibition trapping region  $\mathcal{T}_\tau^I$  by

$$\mathcal{T}_\tau^I = \{(s, \pi) \in \mathcal{I}: \pi > \pi_\tau^I(s) \text{ if } s \in (s_{\tau, \min}^I, s_{\tau, \max}^I)\}, \quad (7.23)$$

then an orbit that lies in the closure of a connected component of  $\mathcal{T}_\tau^I$  at  $\xi = \xi_0$  must remain in that connected component for  $\xi < \xi_0$ . (It might arrive at the right side boundary  $s = 1$  within a finite interval in  $\xi$ .)

### 7.3. Admissible shock waves

We now determine which shock waves have diffusive profiles. Let the shock wave have left state  $(s^-, \pi^-)$ , right state  $(s^+, \pi^+)$ , and speed  $\sigma$ . Recall that  $s^+$  must be distinct from  $s^-$ . We present details of the analysis only in the case  $s^+ < s^-$ ; the case  $s^- < s^+$

is analogous. Also note that, because  $(s^+, \pi^+)$  cannot be a repeller for system (7.2), lemma 7.2 implies that  $\sigma \geq \partial f / \partial s$  at  $(s^+, \pi^+)$  and therefore  $\sigma \geq 0$ . The following propositions treat the three subcases.

**Proposition 7.4.** Assume that  $(s^-, \pi^-)$  lies strictly inside the scanning region and that  $s^+ < s^-$ . Then, if  $\tau > 0$  is sufficiently small, an orbit of system (7.2) leading from  $(s^-, \pi^-)$  to  $(s^+, \pi^+)$  exists if and only if  $\pi^+ = \pi^-$  and

$$\frac{f(s, \pi^+) - f(s^-, \pi^-)}{s - s^-} < \sigma \quad \text{for all } s \in (s^+, s^-). \tag{7.24}$$

Moreover, this orbit is unique and coincides with the portion of the  $\pi^-$ -scanning curve between  $s^+$  and  $s^-$ .

*Proof.* As  $\dot{\pi} = 0$  in the scanning region, any orbit originating at  $(s^-, \pi^-)$  coincides with a portion of the  $\pi^-$ -scanning curve near this point. There are two possibilities: the orbit coincides, near  $(s^-, \pi^-)$ , with a portion where (a)  $s < s^-$  or (b)  $s > s^-$ .

In case (a),  $\dot{s} = h/\varepsilon < 0$  near  $(s^-, \pi^-)$ . Therefore the orbit extends to either (i) a point of  $\overline{\mathcal{S}}$  where  $h = 0$  or (ii) a point on the drainage curve where  $h < 0$ . In situation (i), this point is the termination of the orbit, so that the orbit connects to  $(s^+, \pi^+)$  if and only if  $\pi^+ = \pi^-$ ; also,  $h < 0$  all along the orbit, so that inequality (7.24) holds and the orbit coincides with the portion of the  $\pi^-$ -scanning curve between  $s^+$  and  $s^-$ .

In situation (ii), the Rayleigh line

$$-\sigma(s - s^-) + f - f(s^-, \pi^-) = 0 \tag{7.25}$$

in the  $(s, f)$ -plane must intersect the drainage curve. Associated to the intersection point is a region  $\overline{\mathcal{D}}_\tau$  analogous to the region  $\mathcal{I}_\tau$  of lemma 7.3. Because the orbit reaches a point of  $\overline{\mathcal{D}}_\tau$ , it cannot connect to the equilibrium  $(s^+, \pi^+)$ , according to (the drainage analogue of) the discussion after lemma 7.3.

Similarly, in the case (b),  $\dot{s} = h/\varepsilon > 0$  near  $(s^-, \pi^-)$ , and the orbit extends to either (iii) a point of  $\overline{\mathcal{S}}$ , where  $h = 0$  or (iv) a point on the imbibition curve where  $h > 0$ . In situation (iii), the orbit connects to a point  $(s', \pi^-)$ , where  $s' > s^- > s^+$ , not to  $(s^+, \pi^+)$ . In situation (iv), the orbit reaches a point of  $\overline{\mathcal{I}}_\tau$ , so that it cannot connect to  $(s^+, \pi^+)$ .  $\square$

**Proposition 7.5.** Assume that  $(s^-, \pi^-)$  lies on the imbibition curve and that  $s^+ < s^-$ . Then, if  $\tau > 0$  is sufficiently small, an orbit of system (7.2) leading from  $(s^-, \pi^-)$  to  $(s^+, \pi^+)$  exists if and only if  $\pi^+ \leq \pi^-$  and

$$\frac{f(s, \pi) - f^1(s^-)}{s - s^-} < \sigma \quad \text{for all } s \in (s^+, s^-), \tag{7.26}$$

where  $\pi$  is such that  $(s, \pi)$  lies on the  $\pi^+$ -extended fractional flow curve. Moreover, this orbit is unique and consists of two parts: a curve that ends at a point on the imbibition curve between  $s^1(\pi^+)$  and  $s^-$ , and the portion of the  $\pi^+$ -scanning curve between  $s^+$  and  $s^1(\pi^+)$ .

*Proof.* According to lemma 7.2(ii), any orbit originating at  $(s^-, \pi^-)$  either: (a) coincides, near  $(s^-, \pi^-)$ , with a portion of the  $\pi^-$ -scanning curve where  $s < s^-$ ; (b) enters the region  $\mathcal{I}_\tau$  associated to  $(s^-, \pi^-)$ ; or (c) enters the imbibition trapping region  $\mathcal{T}_\tau^I$ . As in the preceding proof, case (a) entails either that the orbit fails to connect to  $(s^+, \pi^+)$  or that  $\pi^+ = \pi^-$  and the orbit is a connection of the kind described in proposition 7.4. In case (b), the orbit cannot connect to the equilibrium  $(s^+, \pi^+)$ , according to the discussion after lemma 7.3.

In case (c), consider the connected component of the trapping region  $\mathcal{T}_\tau^I$  that contains  $(s^-, \pi^-)$  in its closure. As  $\dot{\pi} \leq 0$  in the imbibition region,  $(s^-, \pi^-)$  must be the top equilibrium in the closure. According to the discussion after lemma 7.3, any orbit originating at  $(s^-, \pi^-)$  and entering  $\mathcal{T}_\tau^I$  either: (i) reaches the imbibition curve at a point where  $\dot{s} < 0$ ; (ii) reaches the barrier curve  $\Gamma_\tau^I$  at a point on  $\partial\mathcal{I}_\tau$ ; or (iii) tends to the bottom equilibrium in the closure. In situation (i), the orbit continues as a portion of a scanning curve, and it connects to  $(s^+, \pi^+)$  if and only if  $(s^+, \pi^+)$  lies on the scanning curve and inequality (7.26) holds. In situation (ii), the orbit cannot connect to  $(s^+, \pi^+)$ . Finally, in situation (iii), the orbit connects to  $(s^+, \pi^+)$  if and only if  $(s^+, \pi^+)$  is the bottom equilibrium, i.e.,  $(s^+, \pi^+)$  lies on the imbibition curve and inequality (7.26) holds.

As  $\tau \rightarrow 0^+$ , the trapping region  $\mathcal{T}_\tau^I$  shrinks, so that the portion of an orbit contained in this region approaches the portion of the imbibition curve between  $\pi^-$  and  $\pi^+$ .  $\square$

*Remark 7.6.* Because the portion of a connecting orbit that lies outside the scanning region approaches the imbibition curve as  $\tau \rightarrow 0^+$ , the admissibility of a shock wave is independent of the choice for the extension of the scanning curves outside the scanning region.

**Proposition 7.7.** Assume that  $(s^-, \pi^-)$  lies on the drainage curve and that  $s^+ < s^-$ . Then, if  $\tau > 0$  is sufficiently small, no orbit of system (7.2) leading from  $(s^-, \pi^-)$  to  $(s^+, \pi^+)$  exists.

*Proof.* Any orbit originating at  $(s^-, \pi^-)$  either: (a) coincides, near  $(s^-, \pi^-)$ , with a portion of the  $\pi^-$ -scanning curve where  $s > s^-$ ; (b) enters the region  $\mathcal{D}_\tau$  associated to  $(s^-, \pi^-)$ ; or (c) enters the drainage trapping region  $\mathcal{T}_\tau^D$ . In case (a), the orbit reaches a point  $(s', \pi^-) \in \overline{\mathcal{S}}$  where  $h = 0$ ; since  $s'$  must exceed  $s^-$ , this point cannot be  $(s^+, \pi^+)$ . In case (b), the orbit remains in  $\overline{\mathcal{D}_\tau}$  and therefore cannot connect to  $(s^+, \pi^+)$ . In case (c),  $(s^-, \pi^-)$  must be the bottom equilibrium of the closure of the connected component of  $\mathcal{T}_\tau^I$  that contains  $(s^-, \pi^-)$  in its closure, and an argument analogous to the one in the preceding proof shows that the orbit cannot connect to  $(s^+, \pi^+)$ .  $\square$

To summarize, these foregoing results and their counterparts for  $s^- < s^+$  establish the following theorem.

**Theorem 7.8.** Consider a shock wave with left state  $(s^-, \pi^-)$ , right state  $(s^+, \pi^+)$ , and speed  $\sigma$ ; also let  $\eta = \pi^+$ . This shock wave has a diffusive profile if and only if the left

state lies on the  $\eta$ -extended fractional flow curve, i.e.,  $f(s^-, \pi^-) = F^\eta(s^-)$ , and the Oleřnik criterion is satisfied with respect to this curve:

$$s^+ < s^- \quad \text{and} \quad \frac{f(s, \pi) - f(s^-, \pi^-)}{s - s^-} < \sigma$$

whenever  $s \in (s^+, s^-)$  and  $f(s, \pi) = F^\eta(s)$  (7.27)

or

$$s^- < s^+ \quad \text{and} \quad \frac{f(s, \pi) - f(s^-, \pi^-)}{s - s^-} > \sigma$$

whenever  $s \in (s^-, s^+)$  and  $f(s, \pi) = F^\eta(s)$ . (7.28)

Moreover, any portion of the profile that lies in the imbibition (respectively, drainage) region tends to the imbibition (respectively, drainage) curve as  $\tau \rightarrow 0^+$ .

In particular, the water saturation increases upon passage of an admissible imbibition or scanning-to-imbibition shock wave, and it decreases upon passage of an admissible drainage or scanning-to-drainage shock wave.

*Remark 7.9.* In [18], Liu investigated two-component systems of conservation laws with relaxation. Just as in the SHMR, the zero relaxation-time limit is formally a scalar conservation law, known as the equilibrium system. Liu identified an important stability criterion: the characteristic speed of the equilibrium system should lie between the two characteristic speeds of the “frozen” system. This is the subcharacteristic criterion. The SHMR, however, violates this criterion: the equilibrium characteristic speeds  $df^I/ds$  for imbibition waves and  $df^D/ds$  for drainage waves exceed the frozen characteristic speed  $\partial f^S/\partial s$  for scanning waves. This violation of the subcharacteristic criterion is reflected in the formal Chapman–Enskog analysis of section 6, where it was found that the relaxation term gives rise to diffusion terms with negative coefficients ( $-\nu^I$  and  $-\nu^D$ ). In the SHMR, these negative coefficients are balanced by the diffusion coefficient  $\varepsilon$  arising from capillarity. Likewise, the geometry of scanning, imbibition, and drainage curves that entails the violation of the subcharacteristic criterion is what allows the construction of the loop solutions associated with the nonuniqueness of solutions in the SHM discussed in section 4.

## 8. Stationary waves

Because the scanning, imbibition, and drainage fractional flow functions are strictly increasing, a horizontal line drawn in the  $(s, f)$ -plane intersects an  $\eta$ -extended fractional flow curve at most once. Therefore a corollary of theorem 7.8 is that a stationary discontinuity for the SHM fails to admit a diffusive profile in the SHMR. In other words, a stationary discontinuity cannot be regarded as an admissible shock wave. However, continuous stationary waves exist for the SHMR, as we now demonstrate.

A stationary solution  $s(x, t) = \hat{s}(x)$  and  $\pi(x, t) = \hat{\pi}(x)$  of equation (5.2) must satisfy

$$f(\hat{s}, \hat{\pi}) = \varepsilon \frac{d\hat{s}}{dx} + \text{const.} \quad (8.1)$$

The hysteresis parameter  $\hat{\pi}$  is unrestricted by equation (5.3), but we assume it to be a continuous function of  $x$ . For simplicity, we also assume that  $\pi(x) = \pi^-$  for  $x < -a$  and  $\pi(x) = \pi^+$  for  $x > a$ , where  $a > 0$ . We seek a solution such that  $\hat{s}(x) \rightarrow s^\pm$  as  $x \rightarrow \pm\infty$ , with  $(s^-, \pi^-)$  and  $(s^+, \pi^+)$  being two states in  $\overline{\mathcal{S}} \setminus \{(0, 0), (1, 1)\}$ . For a stationary solution with this asymptotic behavior to exist, we must have that

$$f(s^-, \pi^-) = f(s^+, \pi^+), \quad (8.2)$$

the common value being the constant appearing in equation (8.1).

In the interval  $x > a$ , equation (8.1) is a scalar autonomous ordinary differential equation:

$$\varepsilon \frac{d\hat{s}}{dx} = f(\hat{s}, \pi^+) - f(s^+, \pi^+). \quad (8.3)$$

Since  $\partial f / \partial s > 0$  at  $(s^+, \pi^+)$ , the equilibrium  $s^+$  is a repeller, so that the only solution that approaches it is the constant solution  $\hat{s}(x) \equiv s^+$ . In contrast, the equation

$$\varepsilon \frac{d\hat{s}}{dx} = f(\hat{s}, \pi^-) - f(s^-, \pi^-) \quad (8.4)$$

holding in the interval  $x < -a$  has a one-parameter family of solutions such that  $\hat{s}(x) \rightarrow s^-$ . These solutions lie along the  $\pi^-$ -scanning curve.

In the interval  $-a < x < a$ , the nonautonomous equation

$$\varepsilon \frac{d\hat{s}}{dx} = f(\hat{s}, \hat{\pi}) - f(s^+, \pi^+) \quad (8.5)$$

can be solved subject to the endpoint condition

$$\hat{s}(a) = s^+. \quad (8.6)$$

In certain circumstances, the solution of this initial-value problem remains within the scanning region throughout the interval  $-a < x < a$ . In this case, the point  $(\hat{s}(-a), \hat{\pi}(-a))$  lies on the  $\pi^-$ -scanning curve and  $\hat{s}(-a)$  provides an endpoint condition that uniquely determines the solution of equation (8.4) such that  $\hat{s}(x) \rightarrow s^-$ . Thus we obtain a continuous stationary wave.

More information about this solution can be obtained by considering the limit of a small diffusion coefficient  $\varepsilon$ . For this purpose, we assume that  $\hat{\pi}$  is  $C^1$ . Let  $\hat{s}_0(x)$  be the saturation such that the fractional flow at  $(\hat{s}_0(x), \hat{\pi}(x))$  coincides with  $f(s^-, \pi^-) = f(s^+, \pi^+)$ ; in other words, let  $(\hat{s}_0(x), \hat{\pi}(x))$  map to the horizontal line in the  $(s, f)$ -plane that connects  $(s^-, f(s^-, \pi^-))$  to  $(s^+, f(s^+, \pi^+))$ . If we express  $\hat{s}$  in terms of a formal asymptotic expansion

$$\hat{s} = \hat{s}_0 + \varepsilon \hat{s}_1 + O(\varepsilon^2) \quad (8.7)$$

as  $\varepsilon \rightarrow 0^+$ , then equation (8.1) yields that

$$\frac{d\hat{s}_0}{dx} = \frac{\partial f}{\partial s}(\hat{s}_0, \hat{\pi})\hat{s}_1 + O(\varepsilon). \tag{8.8}$$

Noting that

$$\frac{\partial f}{\partial s}(\hat{s}_0, \hat{\pi})\frac{d\hat{s}_0}{dx} + \frac{\partial f}{\partial \pi}(\hat{s}_0, \hat{\pi})\frac{d\hat{\pi}}{dx} = 0, \tag{8.9}$$

we find that

$$\hat{s}_1 = -\frac{\partial f/\partial \pi}{(\partial f/\partial s)^2} \frac{d\hat{\pi}}{dx} + O(\varepsilon). \tag{8.10}$$

In other words,  $\hat{s}_1$  equals a term independent of  $\varepsilon$  plus higher order terms. This formal analysis suggests that, as  $\varepsilon \rightarrow 0^+$ , the stationary wave profile  $(\hat{s}, \hat{\pi})$  approaches the profile that corresponds to the horizontal line in the  $(s, f)$ -plane connecting  $(s^-, f(s^-, \pi^-))$  to  $(s^+, f(s^+, \pi^+))$ .

### 9. The Corrected Upstream Scheme

Let us describe a modification of the explicit upstream finite difference method that numerically approximates the Scanning Hysteresis Model defined by equations (4.2)–(4.4).

The Corrected Upstream Scheme proceeds in two stages. Assume that  $s$  and  $\pi$  are known at grid points  $A = (x - \Delta x, t)$  and  $B = (x, t)$  at time  $t$ , and we want to determine them at  $C = (x, t + \Delta t)$ . In the first stage, we compute an intermediate state  $(s^*, \pi^*)$  using the upstream formula:

$$\frac{s^* - s^B}{\Delta t} + \frac{f^S(s^B, \pi^B) - f^S(s^A, \pi^A)}{\Delta x} = 0, \tag{9.1}$$

$$\pi^* = \pi^B. \tag{9.2}$$

Using elementary considerations, one may verify that  $s^* \in [0, 1]$  provided that

$$\Delta t \leq \Delta x \left[ \max \left\{ \sup_{s \in [0,1]} \frac{df^I}{ds}(s), \sup_{s \in [0,1]} \frac{df^D}{ds}(s), \sup_{(s,\pi) \in \bar{\mathcal{S}}} \frac{\partial f}{\partial s}(s, \pi) \right\} \right]^{-1}. \tag{9.3}$$

In the second stage, we compute  $(s^C, \pi^C)$  from  $(s^*, \pi^*)$  as follows. If  $(s, \pi)$  lies within the scanning region, we set  $(s^C, \pi^C) = (s^*, \pi^*)$ . On the other hand, if  $(s^*, \pi^*)$  lies in the imbibition region, the state at  $C$  is found by projecting  $(s^*, \pi^*)$  onto the imbibition curve, maintaining  $s$  constant. Similarly, if  $(s^*, \pi^*)$  lies in the drainage region, the state at  $C$  is found by projecting  $(s^*, \pi^*)$  onto the drainage curve, maintaining  $s$  constant.

The Corrected Upstream Scheme is motivated by the result that the SHM is the  $\tau \rightarrow 0^+$  limit of the SHMR. Indeed, the second stage is an implementation of Euler's scheme for the ordinary differential equation

$$\frac{\partial \pi}{\partial t} = g(s, \pi), \quad (9.4)$$

where  $s$  is regarded as fixed. For instance, when the intermediate state lies in the imbibition region, the initial-value problem for equation (9.4) can be discretized by

$$\frac{\pi^C - \pi^*}{\Delta t} = \frac{\pi_I(s^*) - \pi^*}{\tau}. \quad (9.5)$$

If we take  $\Delta t = \tau$ , the state  $(s^C, \pi^C) = (s^*, \pi_I(s^*))$  is exactly the projected state.

## 10. Numerical experiments

In this section, we present the results of several numerical simulations. Each initial-value problem was solved in two ways:

- (i) for the Scanning Hysteresis Model of section 3 using the Corrected Upstream Scheme of section 9; and
- (ii) for the Scanning Hysteresis Model with relaxation of section 5 using the linearized Crank–Nicolson scheme.

Refer to appendix A for details concerning the permeability functions  $k_w$ ,  $k^D$ ,  $k^I$ , and  $k^S$  of the test model. For the SHMR,  $\tau = 0.00015$  and  $\varepsilon = 0.001$ .

The first problem is a Riemann problem with initial discontinuity at  $x = 0.3$  separating states  $(s_L, \pi_L) = (0.7, 0.8)$  and  $(s_R, \pi_R) = (0.3, 0.4)$ , which both lie inside the scanning region. The simulation results for the SHM and the SHMR are graphically indistinguishable and are shown in figure 6. By time  $t = 0.3$ , the solution has stabilized to a scale-invariant form. As seen from the saturation profile and the plot in the  $(s, f)$ -plane, the solution comprises (from right to left) a scanning-to-imbibition shock wave from  $R$  to  $B$ , an imbibition rarefaction wave from  $B$  to  $A$ , and a continuous stationary wave from  $A$  to  $L$ . The numerical scheme resolves the traveling wave profile of the scanning-to-imbibition shock wave, so that it appears in the  $(s, f)$ -plot as a scanning curve joining  $R$  to an intermediate point  $C$  on the imbibition curve followed by a traveling wave profile from  $C$  to  $B$ , as expected from the results in section 7.3. (The traveling wave profile is an orbit for equation (7.2) with  $(s^-, \pi^-) = (s_B, \pi_B)$  and  $\sigma$  equal to the slope of the chord from  $R$  to  $B$ .) Also, the stationary wave is not a discontinuity from  $A$  to  $L$ , but rather a continuous wave that deviates slightly from a horizontal line, in conformance with the discussion in section 8.

The initial data for the second problem leads around a loop starting and ending at the imbibition state  $(s_L, \pi_L) = (0.6, 0.6) = (s_R, \pi_R)$ ; it can be regarded as a perturbation of a trivial Riemann problem (i.e., one with coincident left and right state). Nevertheless,

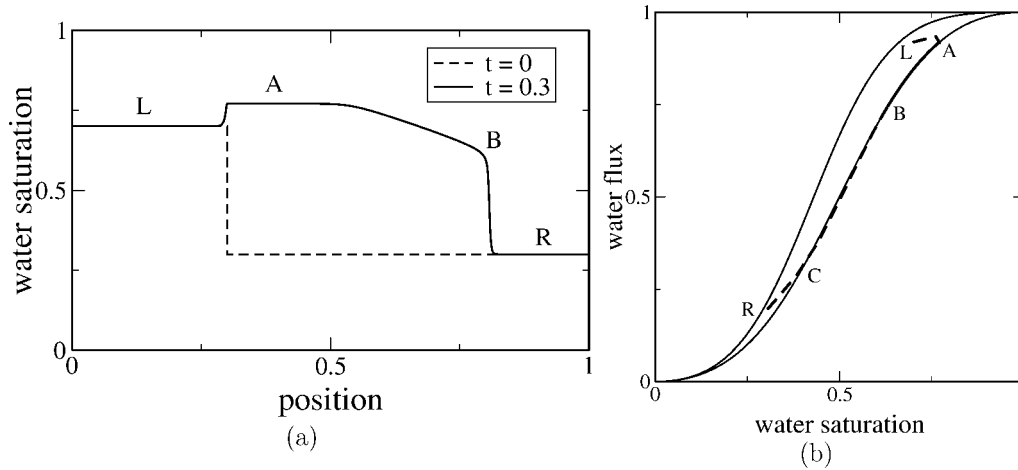


Figure 6. (a) Water saturation profiles at  $t = 0$  and  $t = 0.3$  for a Riemann problem for SHMR. (b) The solution profile at  $t = 0.3$  (dashed and bold curves) plotted in the  $(s, f)$ -plane.

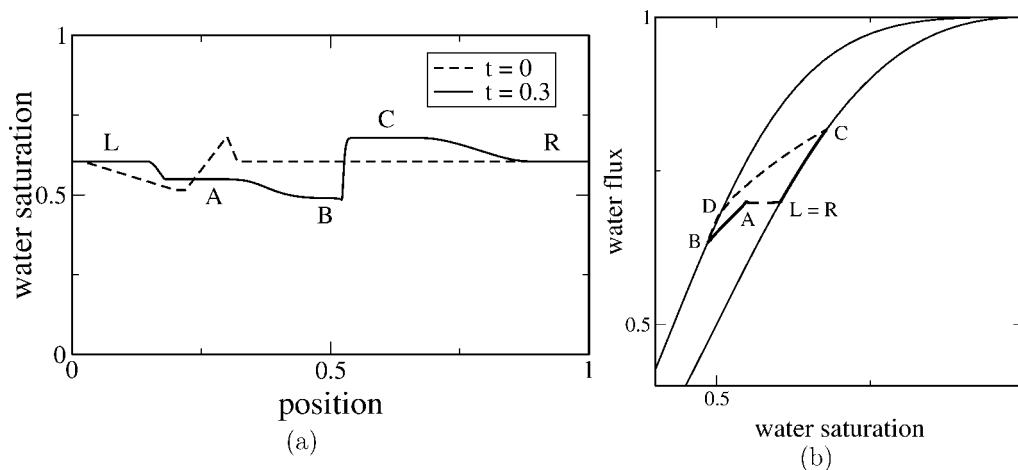


Figure 7. (a) Water saturation profiles at  $t = 0$  and  $t = 0.3$  for a Cauchy problem for SHMR. (b) The solution profile at  $t = 0.3$  (dashed and bold curves) plotted in the  $(s, f)$ -plane.

the time-asymptotic solution is not, as one might expect, a set of decaying waves superimposed on a constant background. Again the simulation results for the SHM and the SHMR are graphically indistinguishable. Figure 7 shows the solution at an intermediate time,  $t = 0.3$ , when there are four waves: an imbibition rarefaction wave from  $R$  to  $C$ , an imbibition-to-drainage shock wave from  $C$  to  $B$ , a scanning rarefaction wave from  $B$  to  $A$ , and a continuous stationary wave from  $A$  to  $L$ . The imbibition-to-drainage shock wave is simply the special case of a scanning-to-drainage shock wave with the right state on the imbibition curve. It appears in the  $(s, f)$ -plot as a scanning curve joining  $C$  to an intermediate point  $D$  on the drainage curve followed by a traveling wave profile from  $D$

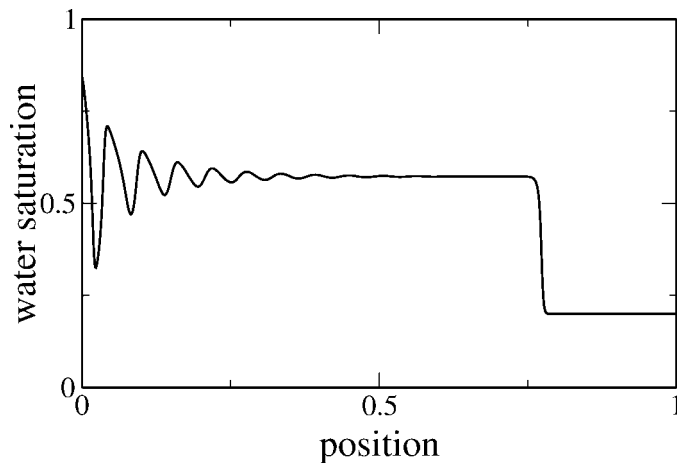


Figure 8. Alternating water–oil injection for two-phase flow without hysteresis.

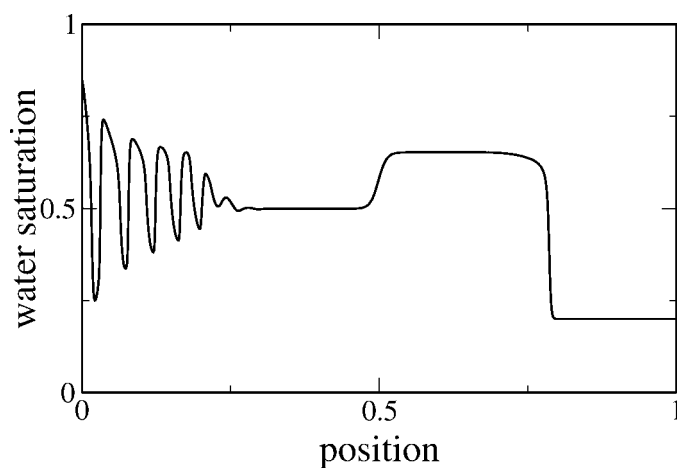


Figure 9. Alternating water–oil injection for the SHMR.

to  $B$ . However, the speed of this shock wave, *viz.*, the slope of the chord from  $C$  to  $B$ , is less than the speed of the scanning rarefaction wave, so that these two waves are interacting; they eventually merge and tend to a scanning shock wave from  $C$  to a point  $E$  preceded by a stationary wave from  $E$  to  $A$ . Thus the scale-invariant time-asymptotic solution of a perturbed trivial Riemann problem can be nontrivial. In other words, there is nonuniqueness of solutions of Riemann problems.

In the third problem, we show the effect of hysteresis on a two-phase flow that is a caricature of an important engineering flow: in analogy with the Water-Alternating-Gas recovery method for three-phase flow, we alternate the injection of water and oil in a two-phase system. We performed two numerical experiments. In the first experiment, shown in figure 8, the two-phase flow model is the standard Buckley–Leverett model,

which exhibits no hysteresis. The second experiment, shown in figure 9, has hysteresis modeled by SHMR. (The SHM gives similar results, but to get close agreement with the SHMR, the grid spacing must be tuned so that numerical viscosity for the CUP scheme is close to the total viscosity of the implicit scheme used for SHMR. However, such tuning is necessary only when the time scale for the oscillating injection is not sufficiently different from the relaxation time in the SHMR.) We see that the bank of injected fluid that is generated in the presence of hysteresis is much larger than without hysteresis. This example illustrates that permeability hysteresis has the potential for having a significant effect on an oil recovery process.

### Acknowledgements

This work was supported in part by: NSF under Grant DMS-9732876; DOE under Grant DE-FG02-90ER25084; CNPq under Grant 451055/00-4; CNPq under Grant 520725/95-6; MCT under Grant PCI 650009/97-5; FINEP under Grants 77.97.0315.00 and 65.990455.00; FAPERJ under Grant E-26/150.936/99; FINEP-CTPETRO under Grant 65.99.0468.00, Subproject 2; and a CNPq Doctoral Fellowship.

We thank Beata Gundelach for careful assistance in preparing the manuscript.

### Appendix A. Test model

The test model used in the figures and numerical simulations presented in this paper is defined by the following assumptions. First, the water permeability is

$$k_w(s) = s^2. \quad (\text{A.1})$$

Second, the drainage oil permeability function is

$$k^D(s) = (1 - s)^3 \quad (\text{A.2})$$

and the imbibition oil permeability function is

$$k^I(s) = (1 - s)^2. \quad (\text{A.3})$$

Third, each scanning curves is a straight line in the  $(s, k)$ -plane:

$$k^S(s, \pi) = a(\pi)s + c(\pi). \quad (\text{A.4})$$

It is convenient to write the constant term as  $c(\pi) = -a(\pi)b(\pi)$ . We adopt the convention that the scanning and imbibition curves coincide for  $s = \pi$ . Then  $k^I(\pi) = k^S(\pi, \pi) = a(\pi)(\pi - b(\pi))$ , so that  $a(\pi) = k^I(\pi)/(\pi - b(\pi))$ , and therefore

$$k^S(s, \pi) = k^I(\pi) \frac{b(\pi) - s}{b(\pi) - \pi}. \quad (\text{A.5})$$

Taking  $b(\pi) = 1/\alpha$  for some  $0 < \alpha < 1$ , we obtain

$$k^S(s, \pi) = \frac{(1 - \pi)^2}{1 - \alpha\pi} (1 - \alpha s). \quad (\text{A.6})$$

With these choices, each scanning permeability curve is a straight line through the point  $(1/\alpha, 0)$  in the  $(s, k)$ -plane. In the figures and numerical simulations,  $\alpha = 1/2$ .

## References

- [1] K. Aziz and A. Settari, *Petroleum Reservoir Simulation* (Applied Science, London, 1979).
- [2] P. Bedrikovetsky, D. Marchesin and P.R. Ballin, A mathematical model for immiscible displacement honouring hysteresis, in: *Fourth Latin American and Caribbean Petroleum Engineering Conf.*, Port of Spain, Trinidad-Tobago (Society of Petroleum Engineers, New York, 1996) pp. 557–575.
- [3] E.M. Braun and R.F. Holland, Relative permeability hysteresis: Laboratory measurements and a conceptual model, *SPE Reservoir Engrg.* (August 1997) 222–228.
- [4] C. Cercignani, *Theory and Application of the Boltzman Equation* (Scottish Academic Press, 1975).
- [5] J. Colonna, F. Brissaud and J.L. Millet, Evolution of capillary and relative permeability hysteresis, *Soc. Petrol. Engrg. J.* (February 1972) 28–38.
- [6] A.J. de Souza, D. Marchesin, P. Bedrikovetsky and P. Krause, A simple model for three phase flow with hysteresis, *Matemática Contemporânea* (2000) submitted.
- [7] F.A.L. Dullien, *Porous Media: Fluid Transport and Pore Structure*, 2nd ed. (Academic Press, New York/Boston, 1992).
- [8] K. Furati, A hysteretic polymer flooding model, Ph.D. thesis, Duke University (1995).
- [9] K. Furati, Effects of relative permeability hysteresis dependence on two-phase flow in porous media, *Transport in Porous Media* 28 (1997) 181–203.
- [10] K. Furati, The solution of the Riemann problem for a hyperbolic system modeling polymer flooding with hysteresis, *J. Math. Anal. Appl.* 206 (1997) 205–233.
- [11] R.E. Gladfelter and S.P. Gupta, Effect of fractional flow hysteresis on recovery of tertiary oil, *Soc. Petrol. Engrg. J.* (December 1980) 508–520.
- [12] Y. Guo, Importance of capillary hysteresis on coreflood experiments, in: *8th European Symposium on Improved Oil Recovery*, Vol. V.I, Vienna, Austria, 15–17 May 1995, pp. 10–17.
- [13] M. Honarpour, L. Koederitz and A.H. Harvey, *Relative Permeability of Petroleum Reservoirs* (CRC Press, Boca Raton, FL, 1986).
- [14] J.E. Killough, Reservoir simulation with history-dependent saturation functions, *Soc. Petrol. Engrg. J.* 37(261) (February 1976) 37–48.
- [15] A.R. Koval, H. Wong and C.J. Radke, A pore level scenario for the development of mixed wettability in oil reservoirs, *AIChE J.* 39(6) (1993) 1072.
- [16] C.S. Land, Calculation of imbibition relative permeability for two- and three-phase flow from rock properties, *Soc. Petrol. Engrg. J.* 243 (June 1968) 149–156.
- [17] R.J. Lenhard and J.C. Parker, A model for hysteretic constitutive relations governing multiphase flow; 2. Permeability-saturation relations, *Water Resour. Res.* 23(12) (1987) 2197–2206.
- [18] T.-P. Liu, Hyperbolic conservation laws with relaxation, *Comm. Math. Phys.* 108 (1987) 153–175.
- [19] D. Marchesin, H.B. Medeiros and P.J. Paes-Leme, A model for two-phase flow with hysteresis, *Contemporary Math.* 60 (1987) 89–107.
- [20] N.R. Morrow, H.T. Lim and J.S. Ward, Effect of crude-oil-induced wettability changes on oil recovery, *SPE Reservoir Engrg.* 89(281) (February 1986).
- [21] W.W. Owens and D.L. Archer, The effect of rock wettability on oil-water relative permeability relationships, *Trans. AIME* 251 (1971) 873–878.